Heavy-Mineral Placer Deposits of the Ute Mountain Ute Indian Reservation, Southwestern Colorado and Northwestern New Mexico

U.S. GEOLOGICAL SURVEY BULLETIN 2061–B

Prepared in cooperation with the Ute Mountain Ute Tribe and the Bureau of Indian Affairs

AVAILABILITY OF BOOKS AND MAPS OF THE U.S. GEOLOGICAL SURVEY

Instructions on ordering publications of the U.S. Geological Survey, along with prices of the last offerings, are given in the current-year issues of the monthly catalog "New Publications of the U.S. Geological Survey." Prices of available U.S. Geological Survey publications released prior to the current year are listed in the most recent annual "Price and Availability List." Publications that may be listed in various U.S. Geological Survey catalogs (**see back inside cover**) but not listed in the most recent annual "Price and Availability List" may no longer be available.

Reports released through the NTIS may be obtained by writing to the National Technical Information Service, U.S. Department of Commerce, Springfield, VA 22161; please include NTIS report number with inquiry.

Order U.S. Geological Survey publications **by mail** or **over the counter** from the offices listed below.

BY MAIL

Books

Professional Papers, Bulletins, Water-Supply Papers, Techniques of Water-Resources Investigations, Circulars, publications of general interest (such as leaflets, pamphlets, booklets), single copies of Earthquakes & Volcanoes, Preliminary Determination of Epicenters, and some miscellaneous reports, including some of the foregoing series that have gone out of print at the Superintendent of Documents, are obtainable by mail from

U.S. Geological Survey, Map Distribution
Box 25286, MS 306, Federal Center
Denver, CO 80225

Subscriptions to periodicals (Earthquakes & Volcanoes and Preliminary Determination of Epicenters) can be obtained ONLY from the

Superintendent of Documents
Government Printing Office
Washington, DC 20402

(Check or money order must be payable to Superintendent of Documents.)

Maps

For maps, address mail orders to

U. S. Geological Survey, Map Distribution
Box 25286, Bldg. 810, Federal Center
Denver, CO 80225

Residents of Alaska may order maps from

U.S. Geological Survey, Earth Science Information Center
101 Twelfth Ave., Box 12
Fairbanks, AK 99701

OVER THE COUNTER

Books and Maps

Books and maps of the U.S. Geological Survey are available over the counter at the following U.S. Geological Survey offices, all of which are authorized agents of the Superintendent of Documents.

- **ANCHORAGE, Alaska**–Rm. 101, 4230 University Dr.
- **LAKEWOOD, Colorado**–Federal Center, Bldg. 810
- **MENLO PARK, California**–Bldg. 3, Rm. 3128, 345 Middlefield Rd.
- **RESTON, Virginia**–USGS National Center, Rm. 1C402, 12201 Sunrise Valley Dr.
- **SALT LAKE CITY, Utah**–Federal Bldg., Rm. 8105, 125 South State St.
- **SPOKANE, Washington**–U.S. Post Office Bldg., Rm. 135, West 904 Riverside Ave.
- **WASHINGTON, D.C.**–Main Interior Bldg., Rm. 2650, 18th and C Sts., NW.

Maps Only

Maps may be purchased over the counter at the following U.S. Geological Survey offices:

- **FAIRBANKS, Alaska**–New Federal Bldg, 101 Twelfth Ave.
- **ROLLA, Missouri**–1400 Independence Rd.
- **STENNIS SPACE CENTER, Mississippi**–Bldg. 3101

Heavy-Mineral Placer Deposits of the Ute Mountain Ute Indian Reservation, Southwestern Colorado and Northwestern New Mexico

By Robert S. Zech, Richard L. Reynolds, Joseph G. Rosenbaum, *and* Isabelle K. Brownfield

GEOLOGIC STUDIES OF THE UTE MOUNTAIN UTE INDIAN RESERVATION

U.S. GEOLOGICAL SURVEY BULLETIN 2061–B

Prepared in cooperation with the Ute Mountain Ute Tribe and the Bureau of Indian Affairs

Numerous small deposits of heavy minerals occur in the Cretaceous Point Lookout Sandstone of the Ute Mountain Ute Indian Reservation

UNITED STATES GOVERNMENT PRINTING OFFICE, WASHINGTON : 1994

U.S. DEPARTMENT OF THE INTERIOR
BRUCE BABBITT, Secretary

U.S. GEOLOGICAL SURVEY
Gordon P. Eaton, Director

For sale by U.S. Geological Survey, Map Distribution
Box 25286, MS 306, Federal Center
Denver, CO 80225

Library of Congress Cataloging-in-Publication Data

Heavy-mineral placer deposits of the Ute Mountain Ute Indian Reservation, Southwestern Colorado and Northwestern New Mexico / by Robert S. Zech ... [et al.].
p. cm. —(Geologic studies of the Ute Mountain Ute Indian Reservation)
(U.S. Geological Survey bulletin ; 2061–B)
Includes bibliographical references (p.).
Supt. of Docs. no.: I 19.3:2061–B
1. Heavy minerals—Ute Mountain Indian Reservation. 2. Placer deposits—Ute Mountain Indian Reservation. I. Zech, R. S. II. Series. III. Series: U.S. Geological Survey bulletin ; 2061–B.
QE75.B9 no. 2061–B
[TN23.9]
557.3 s—dc20
[549.97882] 94–4647
CIP

CONTENTS

FIGURES

TABLES

HEAVY-MINERAL PLACER DEPOSITS OF THE UTE MOUNTAIN UTE INDIAN RESERVATION, SOUTHWESTERN COLORADO AND NORTHWESTERN NEW MEXICO

By Robert S. Zech, Richard L. Reynolds, Joseph G. Rosenbaum, *and* Isabelle K. Brownfield

ABSTRACT

Numerous heavy-mineral placer deposits occur in the upper part of the Upper Cretaceous Point Lookout Sandstone on the Ute Mountain Ute Indian Reservation of southwestern Colorado and northwestern New Mexico. Measured sections and stratigraphic observations at deposit outcrops confirm a foreshore or beach origin of the deposits, and alignment of their exposures defines a northwest-southeast-oriented linear shoreline system. This depositional setting gives the deposits a predictable shape and trend that allows speculation about their subsurface extent. At least five of the known deposits have potential for subsurface extension.

A magnetization study showed that deposits that extend into the subsurface and undiscovered deposits that are covered by less than 20 m of overburden may be located by magnetic surveys. Magnetization of the deposits is provided mainly by detrital titaniferous magnetite concentrated in the centers of the deposits. Magnetite was apparently deposited fairly evenly throughout the deposits, but postdepositional alteration destroyed large quantities of magnetite near the margins of the deposits.

Very good induration due to iron cementation may be the result of humic acids from organic material in the overlying Menefee Formation mobilizing ferrous iron, particularly from titaniferous magnetite. Ferric oxide was then deposited interstitially in the deposits. There are relatively high amounts of titanium and zirconium and lesser amounts of rare earth elements present in the rocks. Semiquantitative analyses of whole-rock samples show that titanium content averages 7.9 percent and may be as much as 21 percent; zirconium content averages 1.5 percent and may reach as much as 6 percent.

INTRODUCTION

In 1986, the Division of Energy and Minerals of the Bureau of Indian Affairs began a resource assessment of the Ute Mountain Ute Indian Reservation at the request of the Ute Mountain Ute Tribe. As part of that program, the U.S. Geological Survey conducted this study of the heavy-mineral deposits on the Reservation. The investigation examined all of the Ute Mountain Ute Indian Reservation (fig. 1) but did not assess any of the known heavy-mineral deposits on the adjacent Navajo Indian Reservation. The objectives of the study included locating deposits on topographic maps and mapping their surficial extent, characterizing the processes that formed the deposits, inferring the presence of additional deposits in the subsurface, testing the feasibility of magnetic methods in locating buried deposits, and determining elements within the deposits. Although assessing the economic potential of the deposits was not part of the study, some economic considerations are discussed.

Because heavy-mineral deposits are present in exposures of the upper part of the Upper Cretaceous Point Lookout Sandstone, which caps many of the mesas in the central part of the Reservation, the extent of heavy-mineral deposits in this area is well known. Field identification is relatively easy because virtually all the deposits are dark-colored, cemented by a ferric-oxide cement, resistant to erosion, and radioactive. However, the true extent of some individual deposits could not be determined due to overburden. In the other parts of the Reservation where the Point Lookout Sandstone is present, deposits may exist but are not known because exposures are only in steep cliffs that greatly limit access. Heavy-mineral deposits probably occur in the subsurface, particularly along the depositional strike to the southeast on the Reservation and in the northern San Juan basin.

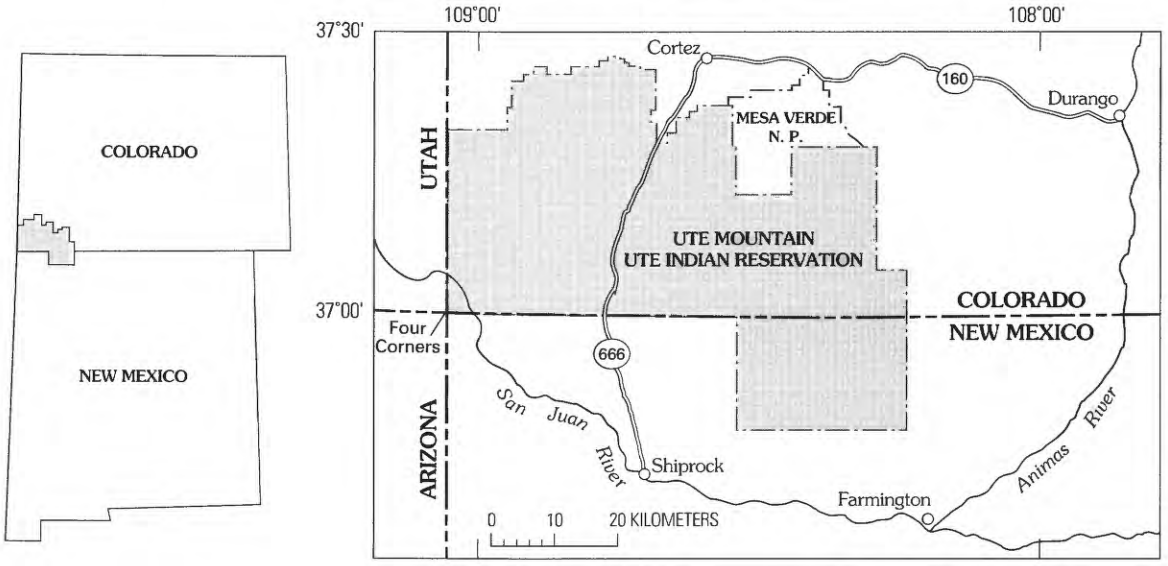

Figure 1. Map of the Four Corners area showing the location of the Ute Mountain Ute Indian Reservation.

ACKNOWLEDGMENTS

We express our appreciation to the Division of Energy and Minerals of the Bureau of Indian Affairs for their support of the research and to the Energy Office of the Ute Mountain Ute Tribe for their cooperation. Thanks also to Robyn Wright Dunbar (Department of Geology, Rice University) for contributing to the fieldwork, and Gary Skipp (U.S. Geological Survey) for sample preparation. Contributions to the magnetization section of this report were made by Allen English, Anne McCafferty, Willie Rivers, and John Karachewski (all from the U.S. Geological Survey). Andrew Grosz of the U.S. Geological Survey reviewed the analytical data. The major-oxide XRF analyses were performed by the U.S. Geological Survey's Clay Petrology Laboratory, Branch of Sedimentary Processes, and Rock Analysis Laboratory, Branch of Central Mineral Resources. Bondar-Clegg & Company of Vancouver, Canada, performed the INAA analyses.

PREVIOUS INVESTIGATIONS

Heavy-mineral placer deposits were discovered in and around the San Juan basin of northwestern New Mexico and southern Colorado as a result of uranium exploration. Airborne gamma-ray radiometric surveys flown by the U.S. Atomic Energy Commission in the mid-1950's detected the radioactive anomalies in the Ute Mountain Ute Reservation. Investigation of these anomalies resulted in a series of U.S. Atomic Energy Commission Preliminary Reconnaissance Reports (PRR) written by Chenoweth (1955a–g), Chenoweth and Carither (1955), and Blagbrough (1955a, b). The reports, which are available in the Field Records Collection of the U.S. Geological Survey Library in Denver, Colo., equate each of the radiometric anomalies with an airborne anomaly (AA) and give each a number. Because these studies served as the basis for most subsequent investigations, this numbering system is used in our study. Table 1 lists the airborne anomaly number and the PRR number for each occurrence.

Murphy (1956) documented the occurrence of heavy-mineral deposits on the Navajo and Ute Mountain Ute Indian Reservations and recommended further study of the economic potential of their titanium, zircon, and radioactive minerals. Chenoweth (1957) summarized the physical and chemical characteristics and stratigraphic distribution of the heavy-mineral deposits in the San Juan basin. This report contains the first substantial discussion of the nonradioactive elements present in the Ute Mountain Ute deposits and their economic potential.

A report by Bingler (1963) on a niobium-bearing deposit in the Upper Cretaceous Gallup Sandstone at Sanostee, N. Mex., in the Navajo Reservation, is the only detailed mineralogical study of a Cretaceous heavy-mineral deposit in the area. He identified the allogenic (zircon, garnet, tourmaline, and ilmenite) and authigenic (barite, leucoxene, and brookite) heavy minerals. Bingler's description of the types, sizes, distribution, and mode of occurrence of minerals in a shoreline heavy-mineral deposit acts as a useful guide for the Ute Mountain Ute Indian Reservation. R.B. O'Sullivan (U.S. Geological Survey, written commun., 1980) briefly examined these deposits as part of the National Uranium Resource Evaluation (NURE) program.

LOCATING THE DEPOSITS

All of the heavy-mineral deposits are in the central and southeastern parts of the Reservation (fig. 2). Except for AA–4 (an occurrence in the Upper Cretaceous Pictured Cliffs Sandstone; Chenoweth and Carithers, 1955), all are found at the top of the Point Lookout Sandstone, which commonly forms cliffs or prominent outcrops. The deposits are better cemented than the surrounding sandstone and form small knolls and ridges along the top of the Point Lookout outcrops. Figure 2 shows a conspicuous northwest-southeast alignment of the deposits that is of considerable help in locating other exposed deposits and inferring areas of potential buried deposits.

When the PRR reports were written, most of the Reservation was not surveyed, and the location descriptions of the deposits relied on reference points such as roads, trails, and windmills. Many of these original reference points have either changed or are missing. Today, topographic maps are available for the area, but there are no section, township, and range lines. Several studies have situated the deposits using projected township and range lines. Unfortunately, these projections are derived from several baselines, and the deposits are still difficult to locate. This study used a combination of maps, descriptions in previous publications, air photos, and scintillometer traverses. Most, but not all, of the previously identified anomalies were found (see table 1). During this search for the deposits, two previously unreported, small deposits were noted (FA–1 and near AA–14; see detailed description of the southern anomaly group). Deposits located in this study are plotted on 1:24,000-scale topographic base maps.

Table 1. List of airborne anomaly numbers and Preliminary Reconnaissance Report (PRR) numbers for the Ute Mountain Ute Indian Reservation.

Airborne anomaly number	PRR number
[1]4	ED-R-431
[1]7	ED-R-435
8, 9	ED-R-433
10, 11	ED-R-434
[1]12	ED-R-436
13	ED-R-451
14	ED-R-452
15	ED-R-453
16, 17, 18	ED-R-437
19, 20	ED-R-438
[1]area near 21	ED-R-473
21	ED-R-439
[1]22	ED-R-454
[1]area near 23	ED-R-472
[1]23	ED-R-454
25	ED-R-471
26	ED-R-426
27	ED-R-469
28	ED-R-468
[1]29	ED-R-467
30	ED-R-466
31	ED-R-465
36	ED-R-440
37	ED-R-441
38	ED-R-493
39	ED-R-494
40	ED-R-495
41	ED-R-496
42	ED-R-497
43	ED-R-498
44	ED-R-499
[2]45	ED-R-500

[1]Not located during this study.
[2]Could not be accessed for this study.

STRATIGRAPHY AND SEDIMENTOLOGY OF UNITS CONTAINING THE DEPOSITS

Condon (1992) and Aubrey (1991) describe the overall stratigraphy of the Reservation. Of most interest to this study are the Point Lookout Sandstone and the overlying Upper Cretaceous Menefee Formation. The Point Lookout is a shoreline deposit and the most areally extensive sandstone unit formed during a regression of the Late Cretaceous sea across the Four Corners area. It interfingers with and overlies offshore marine deposits of the Mancos Shale. Cyclic transgressions and regressions of the paleoshoreline built up a sand deposit to a thickness in excess of 90 m on the Reservation and resulted in a local landward shifting of depositional facies (Zech and Wright Dunbar, 1989; Wright and others, 1989). Figure 3 compares an idealized prograding shoreline with the relationship of the depositional facies that results from one transgressive/regressive cycle, or parasequence. On a basin scale, the Point Lookout parasequences form sets that are indicative of highstand deposition (Van Wagoner and others, 1988). However, late-stage Point Lookout deposition (southwestern Colorado) may be of a lowstand ramp or shelf-margin system tract. Recent observations (Zech and Wright Dunbar, 1989) suggest a basinward shift in coastal facies and the development of a large delta near Durango, Colo., developed above a previously undocumented regional unconformity.

The Chimney Rock area (fig. 4) contains characteristic Point Lookout heavy-mineral deposits. The base of the Point Lookout measured section at Chimney Rock (fig. 5) displays a gradational contact with the underlying Mancos Shale (units 1–6). The section contains at least eight coarsening-upward

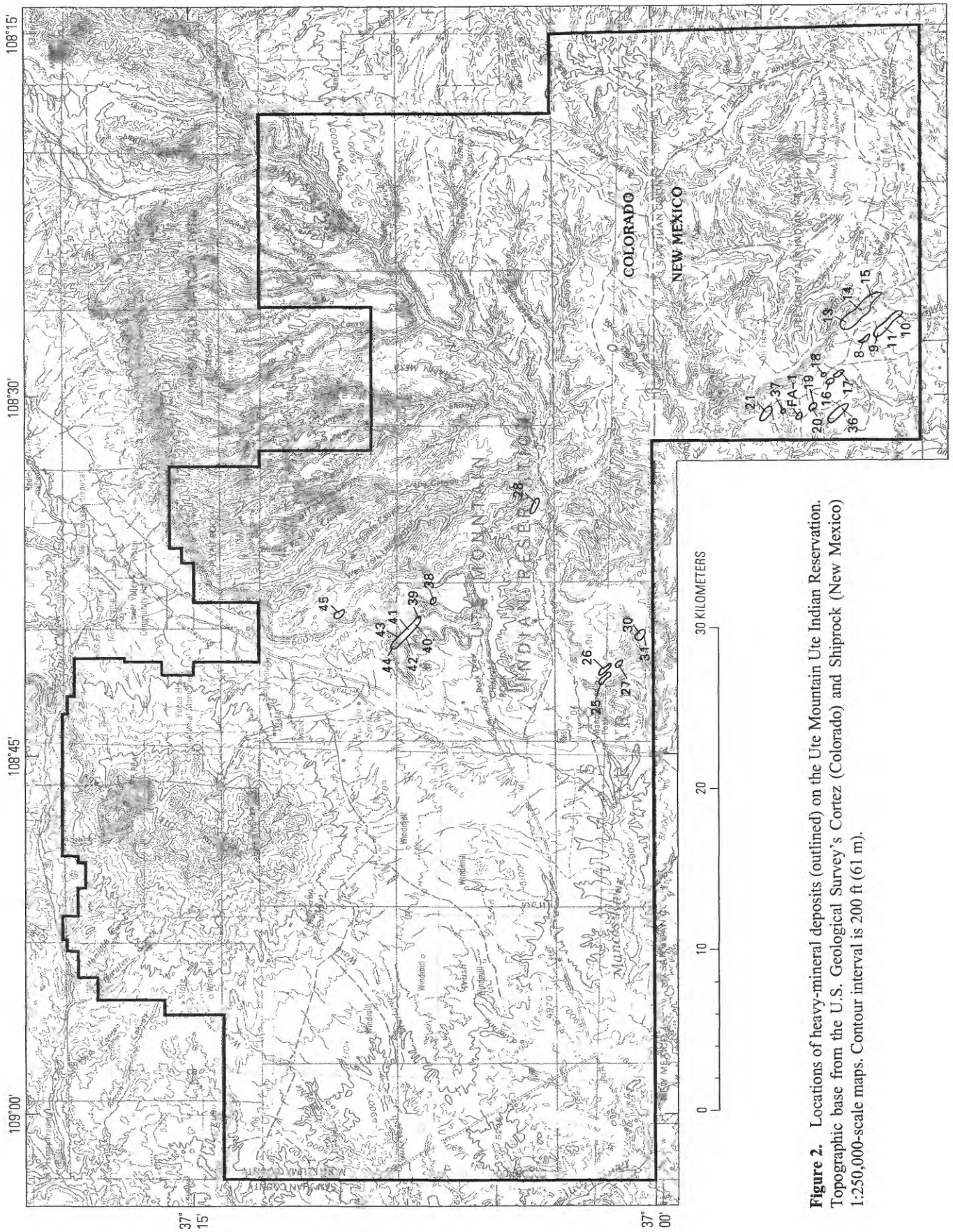

Figure 2. Locations of heavy-mineral deposits (outlined) on the Ute Mountain Ute Indian Reservation. Topographic base from the U.S. Geological Survey's Cortez (Colorado) and Shiprock (New Mexico) 1:250,000-scale maps. Contour interval is 200 ft (61 m).

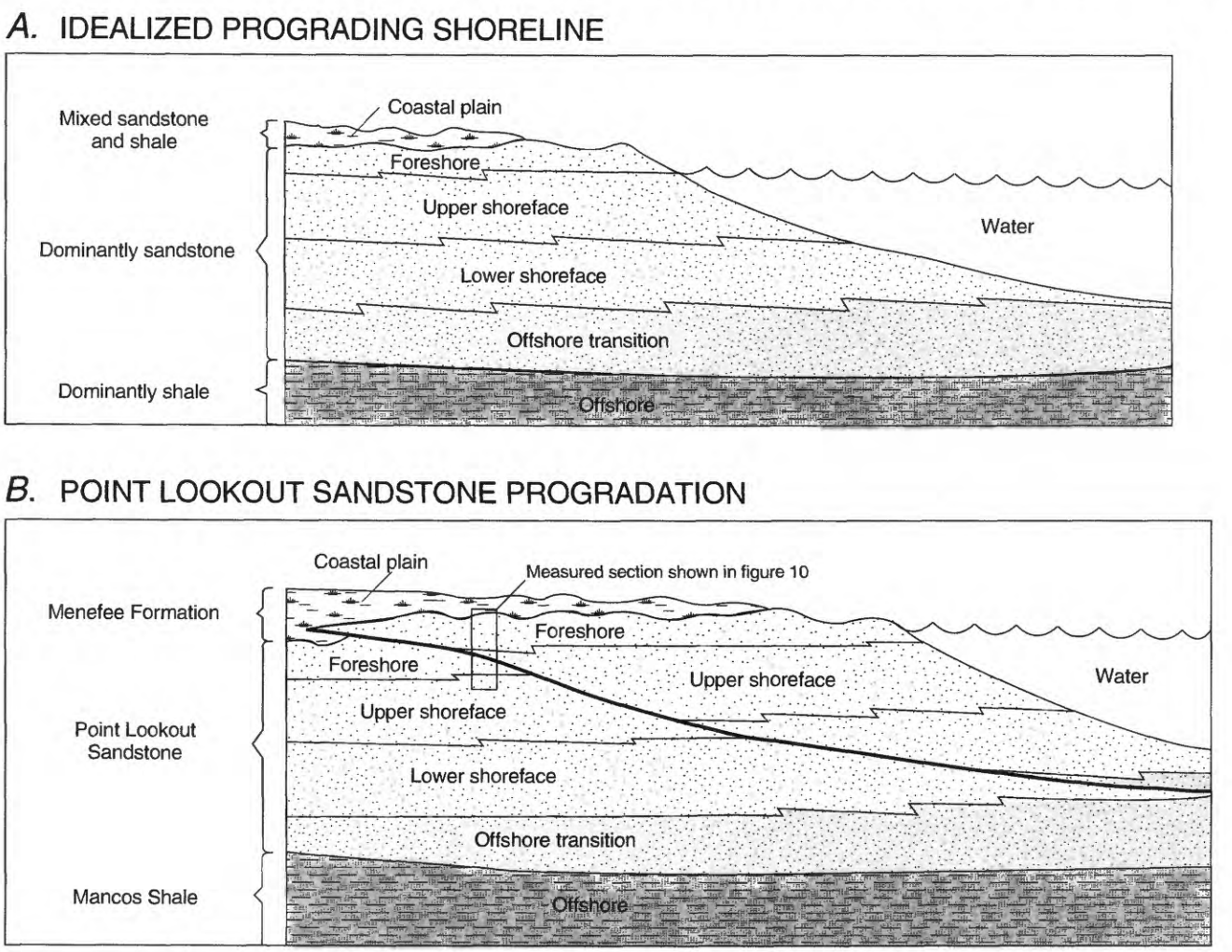

Figure 3. Comparison of an ideal shoreline progradation scheme with a typical parasequence found in the Late Cretaceous Point Lookout Sandstone in the Four Corners area. *A*, uninterrupted deposition results in a seaward buildout of shoreline deposits and a single coarsening-upwards vertical sequence. *B*, a coarsening-upwards vertical sequence is interrupted by a transgression. When deposition reinitiates, all sedimentary facies shift landward. Modified from Wright (1986).

cycles (B–I) within the main sand body, with most of the lower cycles beginning with a basal organic-rich shale or a silty shale. Lenticular siltstone and sandstone interbeds increase in number and thickness vertically until sand dominates the section, forming the base of the Point Lookout cliffs. Maximum grain size falls within the very fine to fine sand range, with individual beds displaying weakly developed, fining-upward trends. Undulatory parallel laminations and hummocky cross-stratification are the most common sedimentary structures, indicating deposition in the inner shelf and distant shoreface environment. The upper cycles contain little shale but are separated from each other by laterally persistent weathering notches. These notches probably represent changes in deposition that would become shale units if traced downdip. The top of the section (unit 25) contains coarser grained sandstone and trough crossbeds of the cliff-forming main body of the Point Lookout, indicating deposition in the middle to upper shoreface.

The higher (foreshore) facies are not preserved in the Chimney Rock section as in most of the Point Lookout, probably due to reworking by the fluvial and tidal processes of the prograding Menefee coastal plain system. However, the facies, some of which contain heavy-mineral deposits, are found in a few areas on the Reservation. Where preserved, the foreshore depositional environment is characterized by gently seaward (northeast)-dipping, even, parallel beds that have lateral continuity ranging from 3 to over 30 m. Generally, the grain size, degree and type of cement, and color of the foreshore beds do not significantly differ from shoreface beds.

The foreshore facies of the Point Lookout interfinger with the Menefee Formation. Fluvial and distributary sandstones of the lower part of the Menefee can be distinguished from sandstones of the Point Lookout on the basis of internal sedimentary structures, a slightly coarser grain size, poorer

Figure 4. Typical exposure of the Point Lookout Sandstone (upper, cliff-forming outcrop) overlying the Mancos Shale (lower, erosional slope) near Chimney Rock, Colo. The Point Lookout measured section in figure 5 is near the right side of the outcrop.

sorting, more carbonaceous material, (generally) more induration, and darker color. Lower coastal plain facies of the Menefee include carbonaceous fluvial and distributary channels, levee and overbank deposits, and coal. In areas where the Point Lookout and Menefee interfinger, any of these deposits may be found under foreshore beds, and fluvial channels of the Menefee commonly scour into or through the foreshore, resulting in sandstone-on-sandstone contact.

ORIGIN AND FIELD CHARACTERISTICS OF HEAVY-MINERAL DEPOSITS

Heavy-mineral deposits on the Ute Mountain Ute Indian Reservation define a linear depositional trend (fig. 2) oriented N. 55°–60° W. that is similar to trends identified by Hollenshead and Pritchard (1961) and Devine (1991). Virtually all of the known deposits occur at the top of the Point Lookout in sediments deposited in a foreshore environment. Interfingering of the Point Lookout foreshore facies with the Menefee coastal plain facies probably led to the initial conclusion in some PRR reports that some of the heavy-mineral deposits were in the Menefee.

Allen and Balk (1954) studied the mineral composition of the Point Lookout and other regressive marine sandstones in the San Juan basin and found them to contain about 1 percent heavy minerals, which is within the normal range for clastic sediments according to A.E. Grosz (U.S. Geological Survey, written commun., 1989). Heavy minerals included tourmaline, garnet, zircon, hematite, ilmenite-magnetite, leucoxene, biotite, and chlorite. The presence of monazite was not investigated. The Allen and Balk (1954) study was in an area where the Point Lookout sandstones were wave dominated (Zech, 1982), as is the case on the Ute Mountain Ute Indian Reservation. One difference between the two areas was the presence of a major(?) fluvial system in the area of the Reservation (Newman, 1982; Zech and Wright Dunbar, 1989). This fluvial system probably originated in a tectonically active source area in southeastern Arizona (Cumella, 1983) and produced the Point Lookout delta near Durango (Zech and Wright Dunbar, 1989). The proximity of the fluvial system most likely increased the general heavy-mineral content of the Point Lookout beach sands.

Normally dispersed heavy minerals in the Point Lookout were concentrated in the foreshore environment by the repeated swash of waves on the beach. When a wave runs up a beach it carries both suspended light grains of sand and a

bedload of heavy grains. Although most of the landward flow of water returns directly to the sea, the return surface flow is smaller and of lesser energy due to percolation of some of the water into beach sands and because of local channelization. The lower energy return water carries back the lighter material but leaves some of the heavy grains in the most landward position, increasing the relative abundance of heavier grains in the foreshore. Repetition of the process concentrates the heavy minerals into a heavy-mineral deposit as the beach grows. Wind may further increase the heavy-mineral content by winnowing the deposits and removing the lighter grains. Although sedimentary structures in the deposits are obscured by a ferric-oxide cement, no eolian sedimentary structures were noted in the deposits on the Reservation. A modern example of heavy-mineral accumulation in the foreshore is shown in figure 6.

Additional information on the formation of heavy-mineral deposits in sedimentary rocks may be found in Mackie (1923), Rittenhouse (1943), Rubey (1933), Stapor (1973), Woolsey and others (1975), and Zenkovich (1967). A good overview (including depositional environments) of most of the known Cretaceous heavy-mineral deposits in the Western Interior was written by Houston and Murphy (1977).

All the deposits are more thoroughly cemented than the surrounding rock and form small, prominent topographic features. Small scarps (as high as the deposit is thick) will generally ring deposits exposed on the tops of knolls or form slope breaks on deposits exposed on hillsides. Most of the deposits are stained black or dark brown from ferric-oxide cement—contrasting in color with the underlying light brown or white Point Lookout Sandstone. A few deposits are only moderately cemented and have a medium-brown color similar to the overlying Menefee channel sandstones. However, these deposits may be easily distinguished from channel sandstones by the increased radioactivity of the heavy minerals.

Weathering of the well-cemented deposits produces abundant small (marble to hand size), black, sharp-edged rock fragments that are generally elongate or flat. Deposits that are nearly covered by eolian material may be easily recognized by these fragments, which are present as a deflation lag on and around the deposit. Because of the resistant nature of the outcrop, these fragments are often the best or only material available for sampling. An unusual (but common on the Reservation) feature in the fragments is slickensides (fig. 7), which are not noted in overlying or underlying rocks. If the elongate or flat nature of the fragments reflects bedding, then the slickensides are at a low angle to bedding. A possible explanation is that leaching of minerals in the deposit and the subsequent induration may have caused a change in the volume of the deposit as a whole, producing slickensides as a method of accommodation.

MAPPING OF HEAVY-MINERAL DEPOSITS

Initially, PRRs were used to locate the airborne anomalies (table 1). Five airborne anomalies (AA–4, AA–7, AA–22, AA–23, and the area near AA–23) could not be located. Airborne anomaly 45 was not visited because of lack of access. For the anomalies that were located, it was necessary to confirm each deposit using a scintillometer because many parts of the Point Lookout (and the lower part of the Menefee) have similar outcrop characteristics to the heavy-mineral deposits. The total gamma-ray count of a heavy-mineral deposit is higher than the surrounding rock because of the increased number of radioactive minerals in the deposit, particularly monazite and zircon. Grosz and others (1989) showed that there is a strong linear relationship between heavy-mineral content and gamma-ray emissions and that gamma-ray activity is an excellent quantitative predictor of the economic heavy-mineral component on a bulk-sample basis. The scintillometer (Geometrics, model GR 101A) was used primarily as a reconnaissance tool. It measured the total gamma-ray flux rate but couldn't distinguish among gamma rays produced by potassium, samarium, isotopes of uranium, or daughter isotopes of thorium. Total gamma radiation was measured in counts per second (cps). An average value for barren Point Lookout Sandstone taken each day was used as a background value. This value ranged from 90 to 120 cps. A deposit was identified as having a multiple radiation count (such as five or six times background) of the average background in the area. The scintillometer was also used to define poorly exposed or covered heavy-mineral deposits that have little surface expression. The edges of such deposits were determined by an abrupt decrease in the counts per second.

Where the exposure was good, the edge of a deposit was easily discernible because the increased iron and calcite cement of the deposit produced either a small escarpment or an abrupt color change. The extent of a deposit was determined by several traverses, and its location was plotted on stereo air photographs. This was transferred to 1:24,000-scale base maps using a Kern PG–2 stereo plotter. The outlines of deposits shown on these location maps are schematic and should not be used to calculate area. The purpose of these maps is to show the general surface shape of the deposits and to show enough detail of the surrounding area to allow easy reference to their locations. Accurate mapping of each deposit would require a scale much larger than 1:24,000.

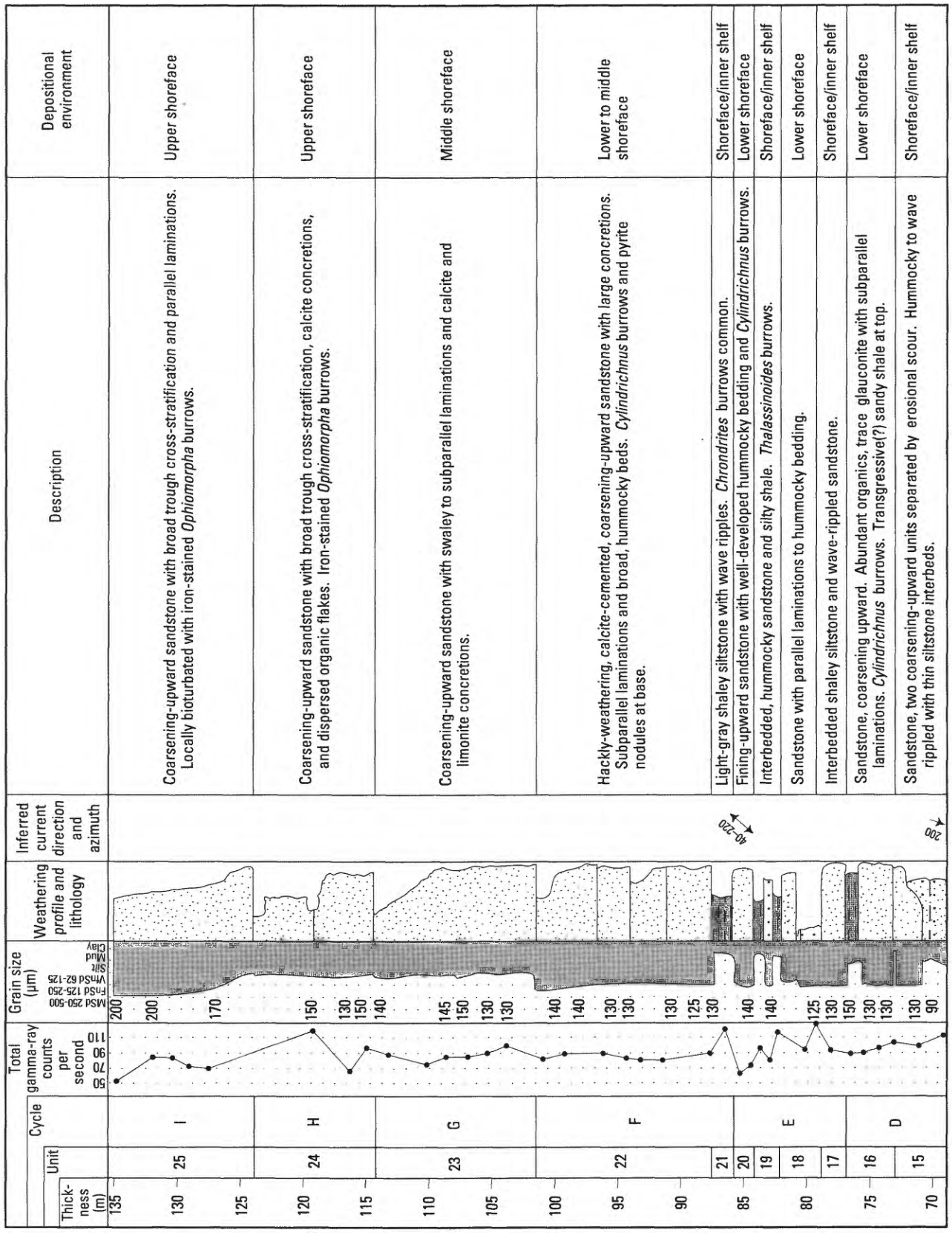
Thick-ness (m)
Unit
Cycle
Total gamma-ray counts per second
Grain size (μm)
MSd 250-500
FnSd 125-250
VfnSd 62-125
Slt/c Mud Clay
Weathering profile and lithology
Inferred current direction and azimuth
Description
Depositional environment
Coarsening-upward sandstone with broad trough cross-stratification and parallel laminations. Locally bioturbated with iron-stained Ophiomorpha burrows.
Upper shoreface
Coarsening-upward sandstone with broad trough cross-stratification, calcite concretions, and dispersed organic flakes. Iron-stained Ophiomorpha burrows.
Upper shoreface
Coarsening-upward sandstone with swaley to subparallel laminations and calcite and limonite concretions.
Middle shoreface
Hackly-weathering, calcite-cemented, coarsening-upward sandstone with large concretions. Subparallel laminations and broad, hummocky beds. Cylindrichnus burrows and pyrite nodules at base.
Lower to middle shoreface
Light-gray shaley siltstone with wave ripples. Chrondrites burrows common.
Shoreface/inner shelf
Fining-upward sandstone with well-developed hummocky bedding and Cylindrichnus burrows.
Lower shoreface
Interbedded, hummocky sandstone and silty shale. Thalassinoides burrows.
Shoreface/inner shelf
Sandstone with parallel laminations to hummocky bedding.
Lower shoreface
Interbedded shaley siltstone and wave-rippled sandstone.
Shoreface/inner shelf
Sandstone, coarsening upward. Abundant organics, trace glauconite with subparallel laminations. Cylindrichnus burrows. Transgressive(?) sandy shale at top.
Lower shoreface
Sandstone, two coarsening-upward units separated by erosional scour. Hummocky to wave rippled with thin siltstone interbeds.
Shoreface/inner shelf
40-220
200

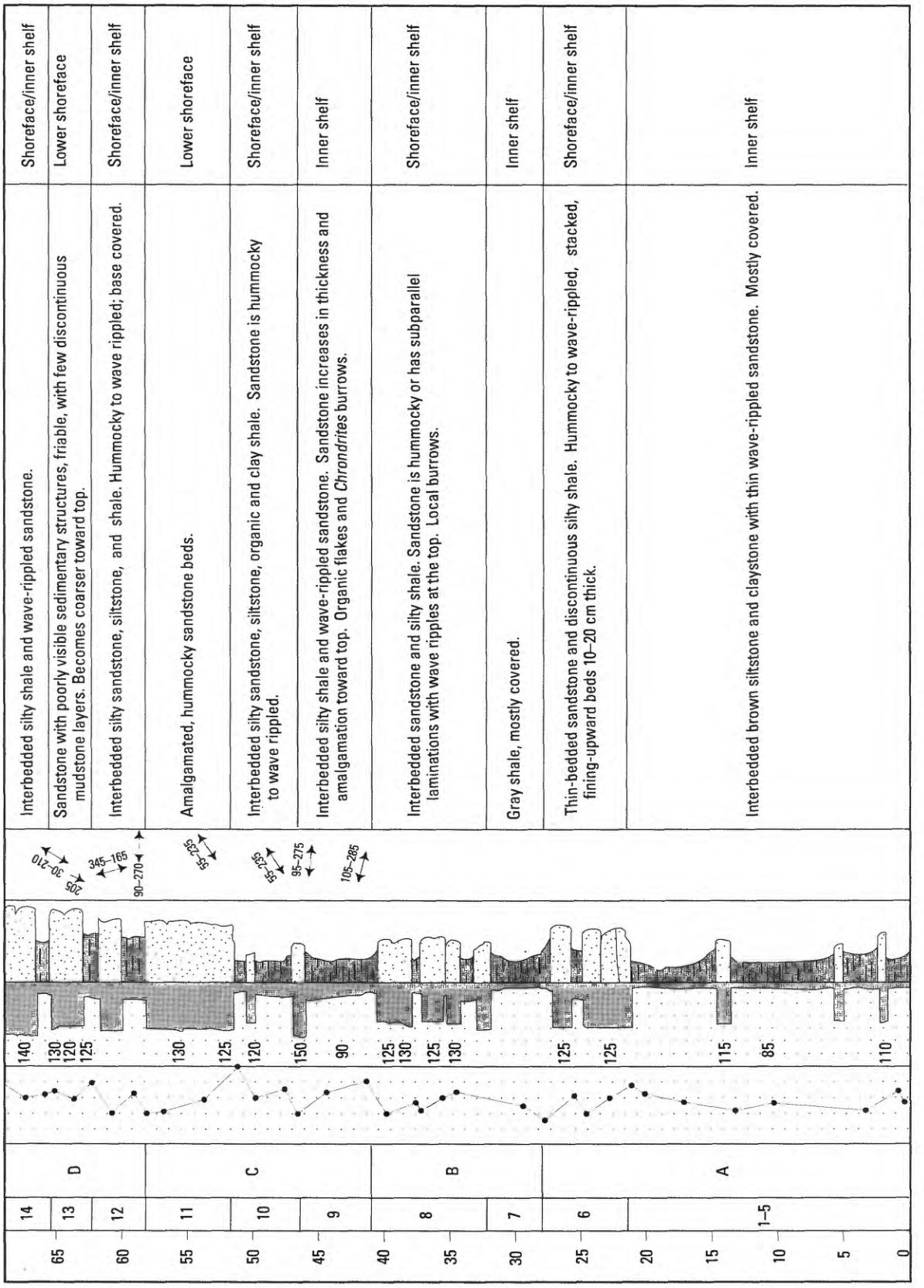

Figure 5. Measured section and geophysical data of the Point Lookout Sandstone near Chimney Rock, Colo. (SW¼SW¼ sec. 28, T. 32 N., R. 17 W.).

Figure 6. Heavy minerals accumulating in the swash zone of the foreshore depositional environment at Mugu Lagoon, Calif. Photograph courtesy of John E. Warme (Colorado School of Mines).

DISTRIBUTION AND PHYSICAL CHARACTERISTICS OF THE DEPOSITS

Most of the heavy-mineral deposits on the Reservation formed along several Upper Cretaceous Point Lookout beaches. The deposits occur in three different geographic areas (fig. 2): the southern group in the New Mexico part of the Reservation (south of lat 37°00′), the central group near the Mancos Trading Post, and the northern group along the north-south-trending cliffs east of Towaoc. This grouping of deposits resulted because the strike of the Point Lookout paleoshorelines combined with present-day structure and erosion limited the area where these deposits could crop out, and because only a few of the regressive beaches developed enough to preserve their foreshore deposits. Only deposits AA–4 and AA–28 fall outside these three groupings. Anomaly AA–4, which was not located during this study, is the only reported heavy-mineral occurrence in a rock unit other than the Point Lookout. The location of AA–4 reported by Chenoweth and Carithers (1955) places it in the Pictured Cliffs Sandstone in sec. 13, T. 14 W., R. 31 N. Anomaly AA–28 is described with the northern group because it is on the same depositional strike and probably formed along the same shoreline.

Figure 2 shows most of the deposits located in this study and indicates that some of the larger deposits include several airborne anomalies. In general, all of the deposits are subparallel and elongate in the direction of the northwest-southeast paleoshorelines. Because of this linearity, it is probable that known deposits link under areas of cover, and undiscovered deposits exist along the identified trends or along parallel trends to the northeast. Unfortunately, a few centimeters of cover will attenuate the characteristic radioactive and magnetic signature of a deposit (Mahdavi, 1964).

SOUTHERN GROUP

The southern group includes airborne anomalies 8–11, 13–21, 36, 37, and FA–1 (fig. 8). This is the largest grouping of airborne anomalies in number and probably in volume. Because the southern group overlies the Verde Oil Field (shown as "Oil Fields" on fig. 2), it is the most easily accessible group on the Reservation. Service roads to the oil wells in the area pass near most of the anomalies, and each anomaly is close to the elevation of nearby access roads.

The southern group formed along at least three separate northwest-southeast-oriented paleoshorelines. Because the shorelines regressed to the northeast, anomaly 36 is the oldest and anomalies 13–15 and 21 are the youngest. Other heavy-mineral occurrences along the three paleoshoreline trends are probable in the subsurface. The most likely areas for additional subsurface deposits are between AA–8 and AA–17 and between AA–13 and AA–21. The magnetic studies, which are discussed in a later part of this report, limit the subsurface potential for heavy-mineral occurrences to the area between AA–8 and AA–21.

AIRBORNE ANOMALIES 8, 9, 10, AND 11

AA–8 and AA–9 are part of a series of separated occurrences at the same stratigraphic level, probably the same bed or within the same foreshore sequence. This is the same set of shorelines that forms AA–10 and AA–11. These occurrences are only 0.3–0.6 m thick, poorly exposed, and discontinuous. However, they are considerably longer than previously reported (Chenoweth, 1955c, d), particularly to the northwest. Small, black, well-cemented, chip- to fist-size rock fragments with total gamma-ray counts of three to eight times normal background characterize most of the surface exposures. The width of each occurrence is unknown because exposures crop out on only one side of a low hill. Because associated deposits AA–10 and AA–11 are wide and the northwest end of AA–8 curves to the northeast, it is possible that most of the occurrences remain covered and may thicken in the subsurface.

AA–10 is stratigraphically lower than AA–11 (fig. 9). As with most of the deposits, a high degree of diagenetic alteration and cementation obscures the sedimentary structures. However, the foreshore origin of AA–10 can be inferred from the gently seaward-dipping, parallel beds below and lateral to the deposit. The heavy-mineral occurrence forms a prominent bench to the southeast that can be traced to the northwest as a dark bed with anomalous gamma-radiation values. An overlying tidal channel locally eroded the heavy-mineral beds (fig. 9, **C**). AA–10 reaches a maximum thickness of 1.5–1.8 m near the center of the deposit and seems to thin rapidly and pinch out(?) at both ends. Some of the apparent thickness change may be due to the increasing cover. The exposed deposit reaches a maximum of 107 m long and 30 m wide. The middle of the deposit is well exposed on the south-facing slope, where a measured section was described (fig. 10).

The two areas of above-background total gamma-ray counts and the corresponding repetition of depositional environments in this measured section indicate that two cycles are present. The top of the lower cycle, about 15 m above the base of the section, was either poorly developed or partially eroded by the subsequent transgression. The mudstone shown in figure 10 at 18 m represents part of the transgressive event shown in figure 3*B*. In figure 3*B*, the location of the measured section detailed in figure 10 is near the landward extent of the transgression where the depositional environments overlap. The foreshore is at the top, underlain by the upper shoreface, the transgressive deposits, and finally the foreshore and upper shoreface.

The lower part of AA–10 is not as well cemented or as dark colored as the upper part. Several samples (AA–10–1 to AA–10–13) were taken at this locality (fig. 10, appendix). The increase in total gamma-ray counts is due to the increase in heavy-mineral content. Samples AA–10–1 to AA–10–5 were barren rock, and AA–10–6 to AA–10–13 were in the heavy-mineral deposit. Occurrences AA–10 and AA–11 were the sites for a feasibility study of magnetic techniques to locate buried heavy-mineral deposits. Results of this effort are described in the section on magnetics.

Figure 7. A rock fragment from a Point Lookout Sandstone heavy-mineral deposit. Note the slickensides.

AA–11 is divided by a small valley (fig. 8). Like many of the heavy-mineral deposits, AA–11 is very well cemented and forms the top of a hill. The upper surface of the deposit is covered by a 15- to 46-cm-thick mixture of angular rock fragments and Holocene eolian sand. Although the sand cover decreases the scintillometer readings over the deposit, a 3–10 times background level was consistently found. The best exposure of the deposit is at the edge of the outcrop on the southwest face of the hill. At this location, the deposit consists of thin, well-cemented, dark beds (containing heavy minerals) separated by thin, moderately well cemented beds of tan sandstone. Even in the best exposures, a pervasive, hard, black ferric-oxide cement obscures the internal sedimentary structures. With the exception of samarium, results from the analysis for this anomaly (see appendix) indicate the sample was from a well-cemented but relatively barren bed.

Rocks below AA–11 are best exposed at the southeast end of the hill where a small cliff exposes (from bottom to top) tidal-channel deposits, a few thin 2.5–5.0 cm coal beds, and the base of a foreshore sequence. The estimated thickness of 0.6–1.2 m is tentative because of poor outcrops and colluvium cover.

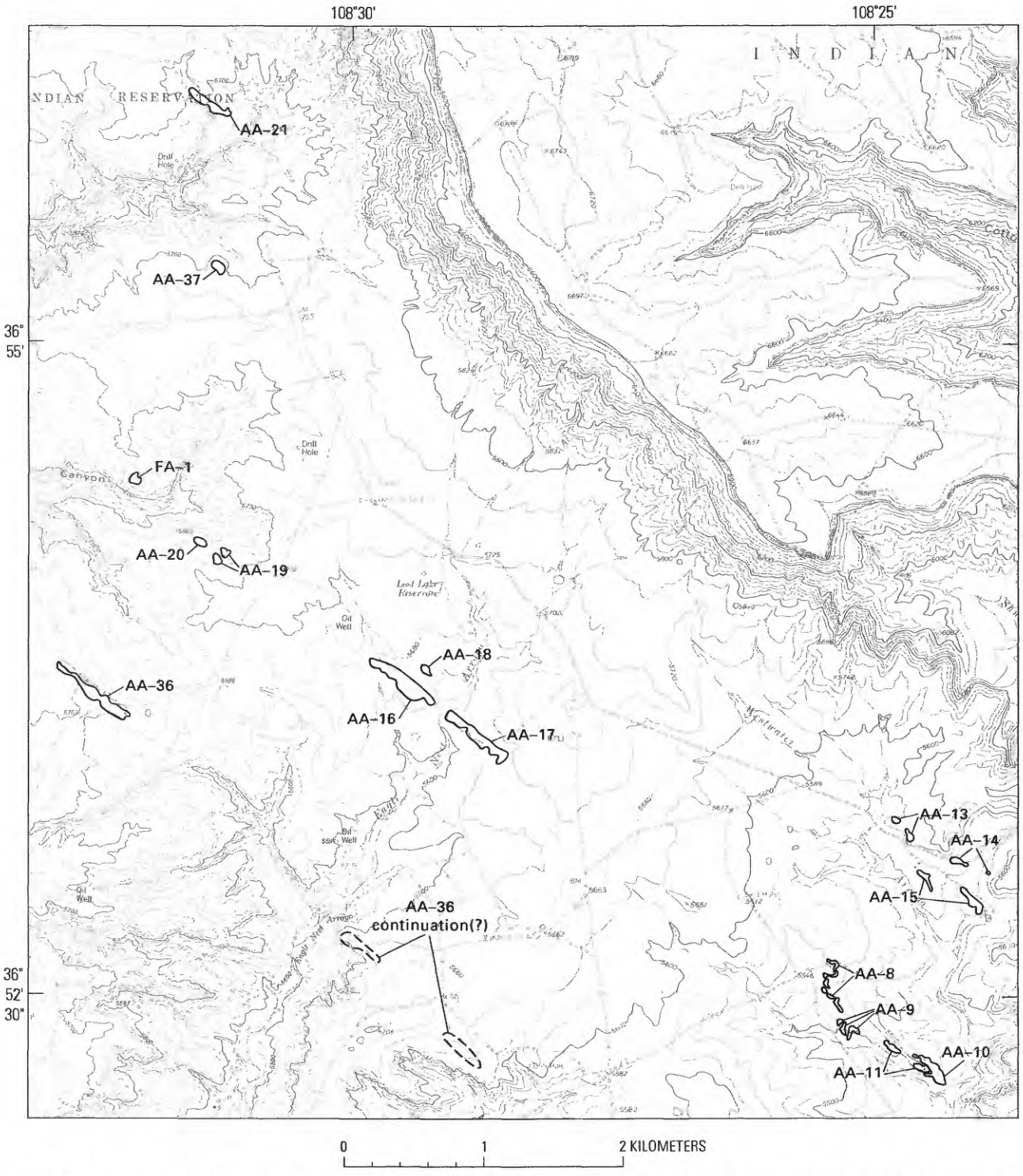

Figure 8. Locations of heavy-mineral deposits in the southern part (New Mexico) of the Ute Mountain Ute Indian Reservation. Topographic base from U.S. Geological Survey Heifer Point (1963) and Palmer Mesa (1983) quadrangles, scale 1:24,000. Contour interval is 40 ft (12.2 m).

Figure 9. Site of heavy-mineral occurrences at AA–10 and AA–11. The dark-colored outcrop on the right (**A**) is AA–10, and AA–11 caps the hill on the left (**B**). The white sandstone (**C**) is a tidal-channel deposit.

AIRBORNE ANOMALIES 13, 14, AND 15

AA–13 consists of two small pods located a few feet north of the main access road for the Verde Oil Field. These pods are thin, less than 0.3–0.6 m, and their total gamma-ray counts are four to five times the background level. AA–13 is on the same strike as AA–14 and AA–15 and probably represents a continuation of the same foreshore. The deposit's thinness is due to its position on the paleoshoreline, which can be determined by the adjacent lithologies and their depositional environments. Above the deposit are the thin sandstone, shale, and coal beds of the Menefee. That part of the Point Lookout immediately below the deposit consists of a 0.6-m-thick, highly bioturbated sandstone bed that rests on a well-developed foreshore sequence (similar to fig. 3*A*). The bioturbated bed indicates the termination of underlying foreshore facies. Therefore, the overlying heavy-mineral-bearing foreshore must be related to a slightly later foreshore sequence. Because foreshores imbricate seaward, AA–13 is probably the landward edge of a younger foreshore. Unless eroded by the Menefee fluvial systems, more and thicker heavy-mineral beds should be found in the subsurface to the northeast.

AA–14 is a few feet south of the main access road to the Verde Oil Field and is identified by an anomalous scintillometer reading (two to eight times background level). Little remains of the deposit. Most of the radiometric anomaly seems to come from erosional remnants consisting of small, black, heavy-mineral-bearing rock fragments that retain a trend approximately parallel to the Point Lookout paleoshoreline. A small radiometric anomaly (two to six times background level) about 3 m in diameter occurs to the southeast along the depositional strike and across a small valley. This occurrence, which was not sampled, is an extension of the AA–14 trend and may be AA–12, which was reported in the area but not located in this study. It is difficult to determine if this small occurrence indicates additional heavy minerals of significant size in the subsurface. Any extension to the southeast projects into an area of increasing overburden.

AA–15 consists of two separate pods at the same stratigraphic level. Like AA–14, small, dark rock fragments cover the surface. Anomaly AA–15 is larger than AA–14 but is very poorly exposed. It is overlain by Holocene eolian and colluvial material that is mixed with the heavy-mineral-bearing rock fragments. Because of the lack of outcrop, no samples were taken and the deposit was defined by the radioactivity measurements. The thickness and width of this deposit could not be determined. The subsurface lateral extent of this deposit may be considerably greater than the surface area shown in figure 8.

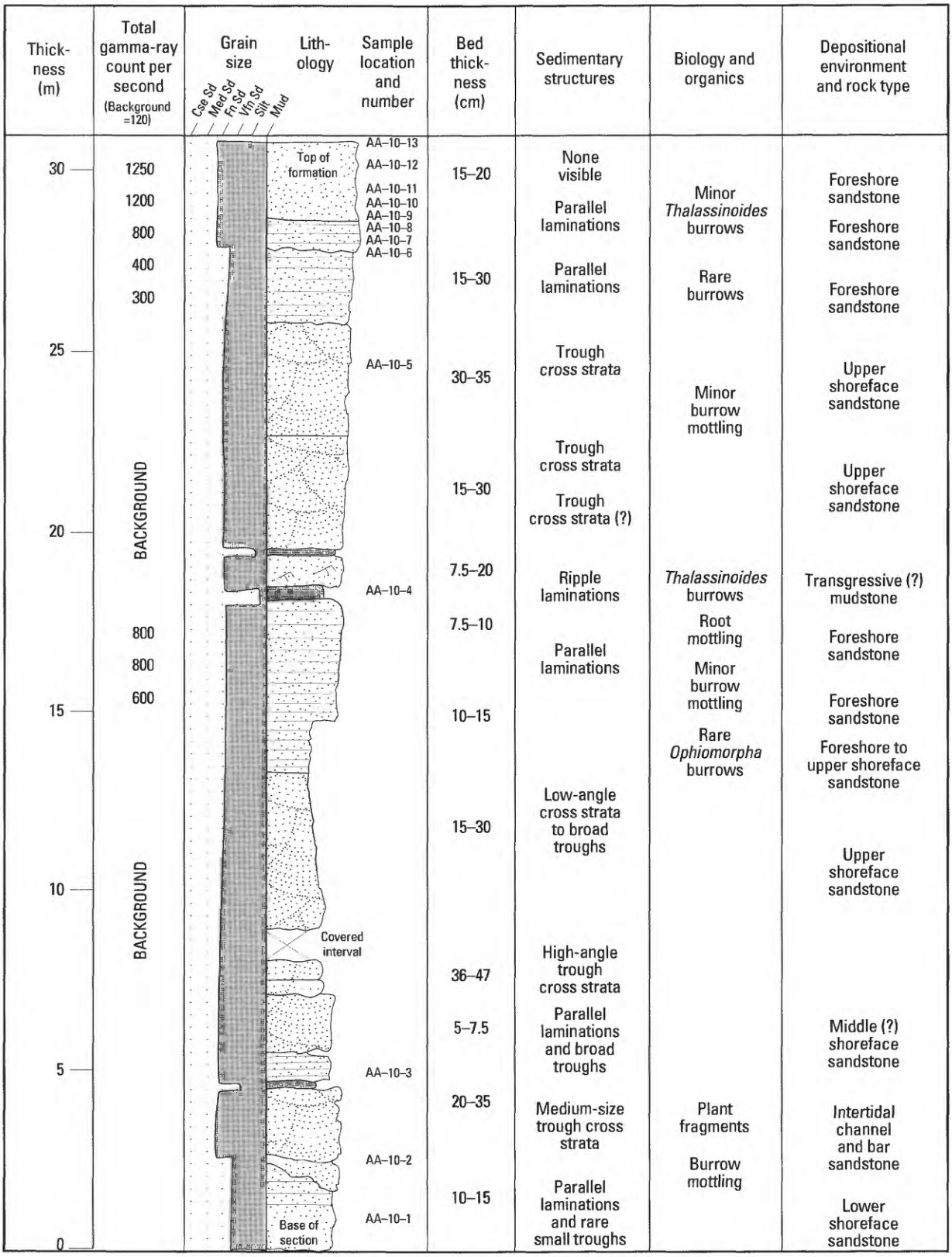

Figure 10. Measured section of the upper part of the Point Lookout Sandstone at location AA–10. This depositional sequence is represented by the rectangular area shown in figure 3*B*.

AIRBORNE ANOMALIES 16, 17, AND 18

Anomalies AA–16, AA–17, and AA–18 are part of the same foreshore deposit that has been split by Eagle Nest Arroyo and a small tributary (fig. 8). These occurrences make up the largest exposed heavy-mineral deposit in the southern group. AA–16 and AA–17 may extend into the subsurface to the northwest and southeast, respectively. Because of their size and probable extension into the subsurface (particularly to the southeast), magnetic investigations were attempted to identify the extent of the covered deposit. Results indicate that the deposit may thin or pinch out to the southeast. The magnetic studies are described in a later section.

Anomaly AA–16, although fairly large, is poorly exposed. Small, dark-colored rock fragments of the heavy-mineral deposit, mixed with Holocene alluvium and eolian sand, cover most of the occurrence. Thickness ranges from 0.3 to 2 m. Total gamma-ray counts ranged from two to eight times background level.

The best exposed anomaly of this group is AA–17, which is located in a small dry drainage about 46 m south to southwest of the end of a drillhole access road. Samples AA–17–1 to AA–17–5 (see appendix) were collected at this locality. AA–17–1 was barren rock from about 1.5 m below the dark-colored deposit. Samples AA–17–2 and AA–17–3, 7.6 m apart, were from the same bed at the base of the deposit. Samples AA–17–4 and AA–17–5 were from 0.3 m and 1 m, respectively, above the base of the deposit. A few of the beds exposed in this locality have only background gamma-ray levels but are well cemented with a dark ferric cement. This could cause some overestimation of the deposit thickness if a scintillometer is not used. The deposit had radiation levels from two to six times the background level and was 0.3-2.3 m thick.

Both AA–16 and AA–17 are about 1.8 m thick where exposed by Eagle Nest Arroyo. Diagenetic cement and slope wash obscure the sedimentary structures within the deposits. A sandstone cliff in the arroyo, just below the deposits, exposes a sedimentary sequence that grades up from upper shoreface to foreshore and tidal channel. The proximity of these environments indicates that the deposit was part of a nearshore environment, probably a foreshore. No seaward extension for AA–17 was found.

Anomaly AA–18 is a relatively thin (0.3–0.9 m) deposit that is probably a seaward extension of AA–16, and it may extend into the subsurface to the northwest. It consists of concentrations of small heavy-mineral-bearing rock fragments and a small outcrop of the deposit at the edge of Eagle Nest Arroyo.

AIRBORNE ANOMALIES 19 AND 20

These anomalies are the erosionally separated remnants of a single foreshore heavy-mineral deposit, probably a northwest extension of AA–16 and AA–17. The surface exposures consist of three closely spaced, small knolls about 30 m in diameter covered with small, dark rock fragments. The heavy-mineral beds are about 1 m thick and have a total gamma-ray count about 6–11 times higher than background. AA–20 does not extend beyond its surface exposure because of erosion. However, AA–19 probably does continue into the subsurface to the southeast. This extension of AA–19 is important because it would indicate the possibility of a much larger occurrence with relatively thin overburden between AA–19 and AA–16, a distance of about 1,520 m (fig. 8).

AIRBORNE ANOMALY 21

Anomaly AA–21 has a surface exposure consisting of mostly ferric-oxide-cemented rock fragments with little exposure along the edge of the nearby canyon (fig. 8). Holocene eolian sand covers much of the upper surface of the deposit. AA–21 is estimated to be 0.6–1.2 m thick, with a total gamma-ray count six to nine times background level. The heavy-mineral deposit may continue into the subsurface to the northwest under unconsolidated colluvium and a thickening overburden of the Menefee Formation. This is the youngest deposit in the southern group, and it does not correlate with the paleoshoreline trend of AA–13, AA–14, and AA–15, which are 7.2 km to the southeast. The upper part of the Point Lookout exposed across the arroyo to the southeast showed no extension of the heavy-mineral trend.

AIRBORNE ANOMALY 36

Anomaly AA–36 is the oldest and longest continuous heavy-mineral deposit exposed in the southern group. It forms the top of a ridge capped by fist-size and smaller rock fragments of the dark-colored, ferric-oxide-cemented heavy-mineral deposit. There is very little outcropping. However, the rock-fragment cover is thinnest along the northern edge of the ridge, where the deposit is 1.0–1.2 m thick and scintillometer values are five to eight times background level. A drillhole marker near the southeast end of the deposit shows the following information: 660FSL, 790 FEL, 32N, 16W, #1 NAV/UTE. The deposit was sampled at each end. As a result of erosion of the surrounding area, there is no possibility of any subsurface extension of the deposit. However, remnants of the deposit may form a prominent northwest-southeast trending ridge about 3,000 m to the southeast (shown in fig. 8).

AIRBORNE ANOMALY 37

The surface expression of AA–37 is similar to the previously described deposits, except that it is smaller and more circular (about 12 m in diameter and about 0.6–0.9 m thick). Some of the foreshore beds beneath the dark, well-cemented deposit register minor increases in total gamma-ray count (one to four times background level) and have a mottled hematite and limonite staining. The upper part of the deposit has a 10–12 times background emissions level. The deposit may extend in the subsurface to the southeast but not to the northwest because of local erosion.

ANOMALY FA–1

This is a small, isolated anomaly that was not reported in the PRRs or in subsequent reports. Like the rest of the southern group, it forms the top of a small knoll, is about 30 m in diameter, and is covered with well-cemented, black-colored rock fragments. Scintillometer values 6–11 times the background level were measured across the deposit. The sample analyzed from this deposit (see appendix) was from a well-cemented but relatively barren bed in the deposit. This anomaly is on the same trend as AA–20, AA–19, and AA–16 and probably represents an extension of the same shoreline deposit. Parallel, laminated seaward-dipping foreshore beds are exposed just beneath the deposit.

CENTRAL GROUP

The central group of anomalies (fig. 11) probably relate to the older shorelines of the southern group, but the distance between the groups makes correlation difficult. Deposits in this group are at the top of the massive Point Lookout Sandstone and are part of an underlying foreshore. Anomalies 25, 27, 30, and 31 are related to the same shoreline and are the oldest in the group. This foreshore sequence is progressively wider to the southeast. In general, the deposits have less of the black to dark-brown color and are more brown to dark-red, indicating a leaching of iron from the deposit (see the petrologic and magnetic descriptions). Like the southern group of deposits, this group is well exposed, has little overburden, and is mostly accessible by existing roads. Except for AA–29, all previously reported anomalies in this group were located. Anomaly AA–29 was described by Chenoweth (1955f) along the Point Lookout-Menefee contact, about 1.5 km east of the eastern border of figure 11. Although the contact was traversed, the anomaly could not be found.

AIRBORNE ANOMALY 25

The deposit at AA–25 is well exposed, about 312 m long by 14 m wide and 0.2–0.8 m thick. A 12-m diameter small erosional remnant of the deposit is present to the southeast. Total gamma-ray counts range from 7 to 15 times background level. Because of the degree of erosion, this trend probably does not continue to the northwest. Anomaly AA–27 is a continuation of this deposit to the southeast. Two samples were taken because of the good exposure, length, and proximity to AA–26.

AIRBORNE ANOMALY 26

Radiometrically and geochemically, AA–26 is the most notable deposit on the Reservation. It is 335 m long and may continue to the northwest in the subsurface. Most of the deposit is 4.5–6.0 m wide and covered by 0.6–0.9 m of unconsolidated Holocene eolian sand. However, where blowouts in the eolian sand expose the deposit, the heavy-mineral deposit is observed to be as much as 12 m wide and 0.6–0.9 m thick. Total gamma-ray counts range from 4 to 30 times background level—the highest value of any of the deposits. Although the gamma-ray emissions for this deposit have a considerable range, the overall values are generally higher than those of other deposits. The highest values are in the southeast part of the deposit. Because of the higher than average gamma-ray values, the deposit was sampled twice. One sample was taken near the northwest end of the deposit and the other near the southeast end. The southeast sample (AA–26–SE) contained almost 6 percent zirconium and 0.1 percent thorium (see appendix). Based on scintillometer traverses and one analysis, this deposit probably contains higher concentrations of zirconium and thorium than any other heavy-mineral deposit on the Reservation.

AIRBORNE ANOMALY 27

This deposit is the least accessible of the central group. The closest access is a road that stops at AA–25, about 914 m to the northwest. AA–27 is part of the same foreshore that forms AA–25 but is separated from it by erosion. AA–27 consists of one main body of heavy minerals (about 137 m long, 10.6 m wide, and 0.6–0.9 m thick) and three smaller bodies (each about 30.4 m long, 10.6 m wide, and 0.3–0.6 m thick). The three smaller remnants are shown in figure 11 as one outlier northwest of the main body. The main body of the deposit has a total gamma-ray count that ranges from 4 to 16 times background level. The smaller bodies range from 4–12 times the background level. Local erosion divides all the deposits.

AIRBORNE ANOMALIES 30 AND 31

These two anomalies represent the same heavy-mineral deposit, the central part of which is covered by Holocene eolian sand. It is an unusual deposit because of its large (76 m) width, which gives it a more rounded than elongate shape in map view. The deposit reaches a maximum length

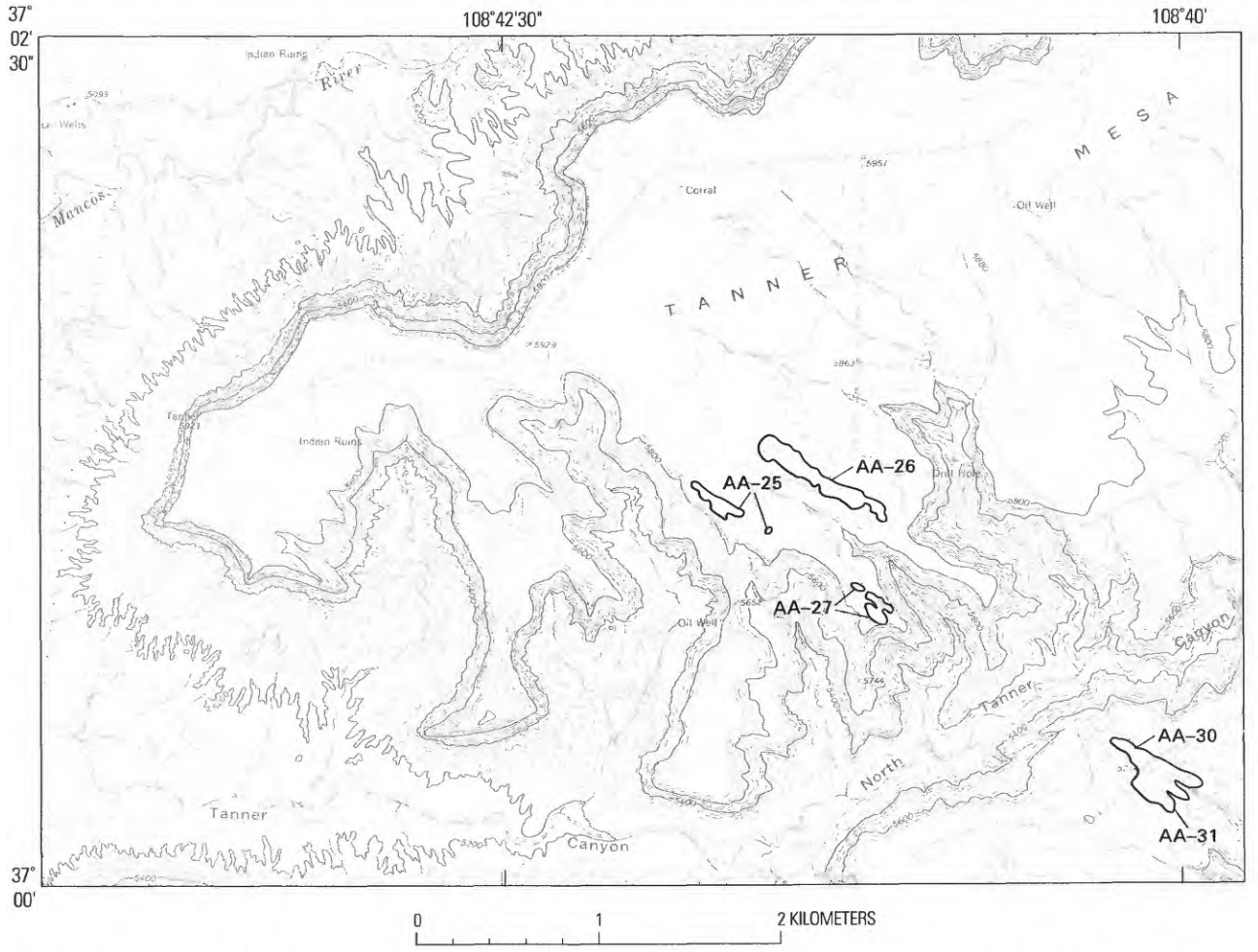

Figure 11. Locations of heavy-mineral deposits in the central part (Colorado) of the Ute Mountain Ute Indian Reservation. Topographic base from U.S. Geological Survey Tanner Mesa (1966) quadrangle, scale 1:24,000. Contour interval is 40 ft (12.2 m).

of 457 m and varies in thickness from 0.6 to 1.1 m. The total gamma-ray counts ranged from 5 to 20 times background level both in the northern (AA–30) and southern (AA–31) outcrops. This deposit is probably related to the same foreshore sequence that forms AA–27 and AA–25. Because of erosion, there is no possible subsurface extension of the deposit on the Reservation. However, this is the same trend that hosts some of the heavy-mineral deposits on the Navajo Reservation, just to the southeast.

NORTHERN GROUP

The northern group of anomalies is shown in figures 12 and 13. The deposits are parts of two separate foreshore sequences that are younger than other heavy-mineral deposits on the Reservation. These two foreshore sequences have very restricted outcrops. However, every outcrop contains a heavy-mineral deposit.

AA–45 (shown only in fig. 2) is the northernmost anomaly on the Reservation. It was not sampled because of restricted access. However, its reported location (Chenoweth, 1955g) indicates that the deposit has minor surface exposure and, if it does extend into the subsurface, it would project into an area of thick overburden.

AIRBORNE ANOMALIES 38–44

These seven anomalies (fig. 12) represent one foreshore sequence and the longest exposed heavy-mineral deposit on the Reservation. Including the width of the three small tributaries that cut through the deposit, the total length from AA–44 to AA–39 is about 2,286 m. Anomaly AA–38, the southeasternmost anomaly of the group, is about 122 m in length and is separated from the other deposits by a 610-m-wide canyon. This is the only anomaly of the group that shows slight iron staining and relatively weak induration. If it was not partially eroded, the total length of the exposed linear deposit would be 3.4 km. Total gamma-ray counts average four to eight times background level. The thickness of this deposit is 0.3–1.2 m.

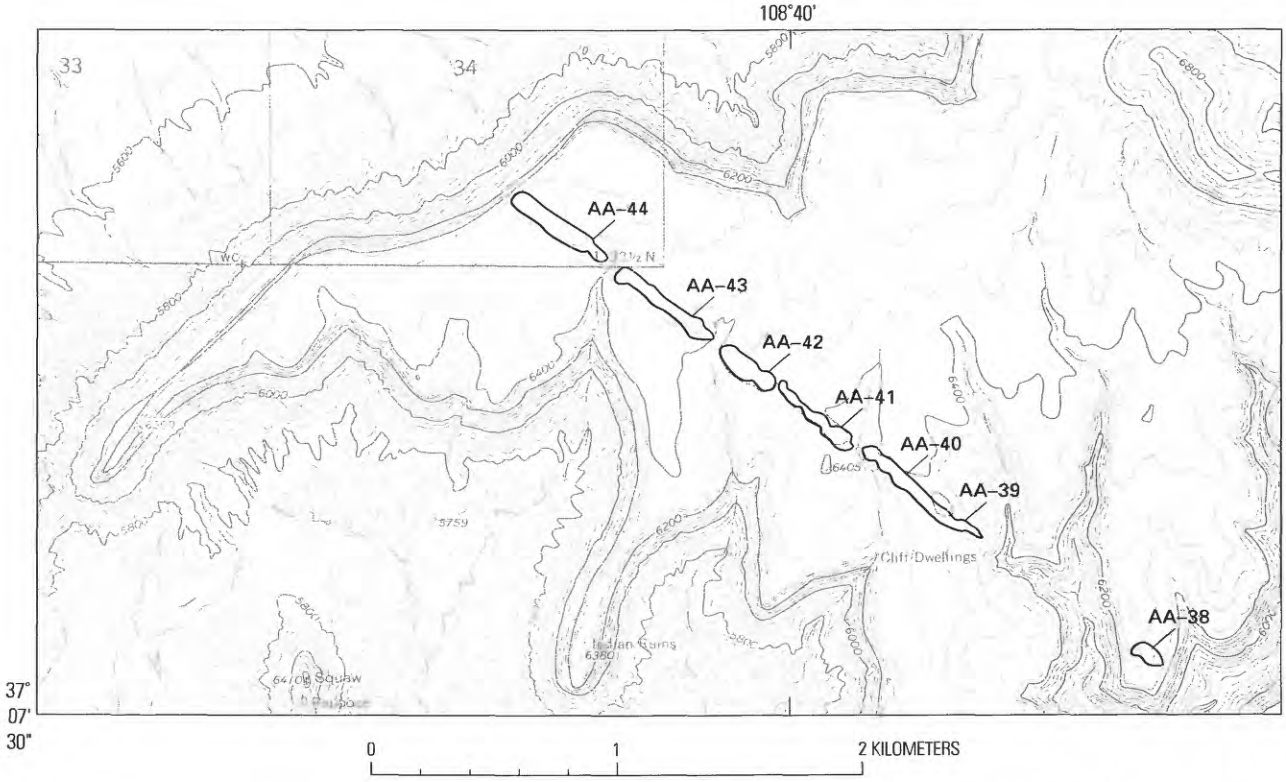

Figure 12. Locations of heavy-mineral deposits in the northern part (Colorado) of the Ute Mountain Ute Indian Reservation. Topographic base from U.S. Geological Survey Towaoc (1966) quadrangle, scale 1:24,000. Contour interval is 40 ft (12.2 m).

An unusable, abandoned road approaches this group of deposits from the north. Rusting tools and minor excavations in the vicinity of AA–41 are evidence of prospecting, possibly for uranium.

AIRBORNE ANOMALY 28

AA–28 may be an extension of the foreshore sequence that produced anomalies 38–44. It is a very small occurrence, about 15 cm thick and 7.6 m in diameter. It is not as dark colored (less ferric cement) as the other deposits, and the total gamma-ray count is two to four times the background level. The down-dip (northwest) continuity cannot be determined because of a thick cover of alluvium from the Mancos River.

MAGNETIC STUDIES

Magnetic analyses of two areas (encompassing anomalies AA–10, AA–11, and AA–17) were undertaken to determine the feasibility of using magnetic methods to locate buried heavy-mineral deposits on the Ute Mountain Ute Indian Reservation. Heavy-mineral deposits typically have higher magnetization than surrounding sediments because they contain concentrations of detrital magnetic minerals. Moreover, the association of magnetite, the most common detrital magnetic mineral, with ilmenite, the primary host for titanium, may link magnetization and titanium content in the heavy-mineral deposits. Anomalies AA–10 and AA–17 were chosen because of their good exposures and potential for extension into the subsurface. AA–11 was included because of its proximity to AA–10.

The magnetic studies consisted of: (1) measurement of the total magnetic field along ground traverses over and between exposed deposits; (2) upward continuation of a total-field profile from an exposed deposit to determine the expected magnetic signals from the deposit at different burial depths; (3) measurements of magnetic susceptibility of the deposits at the outcrops to map the distributions of magnetic minerals in the deposits; (4) laboratory measurements of magnetic susceptibility and remanent magnetization of samples taken in and adjacent to heavy-mineral deposits; and (5) petrologic study and rock magnetic tests to identify the magnetic minerals in the deposits and to explain variations in magnetic properties. The results of this investigation showed that these methods can be used to locate deposits similar to AA–10 if they are buried less than 20 m deep and that magnetization is dominated by authigenic ferric-oxide minerals at the margins and by detrital magnetite and possibly titanohematite in the interiors of the deposits.

Many of the sample sites for the magnetic studies coincide with the sample sites for the geochemical tests. They also share the same sample number, such as AA–17–1. Magnetic-analyses samples that do not share the same sample site begin with the prefix 7UM.

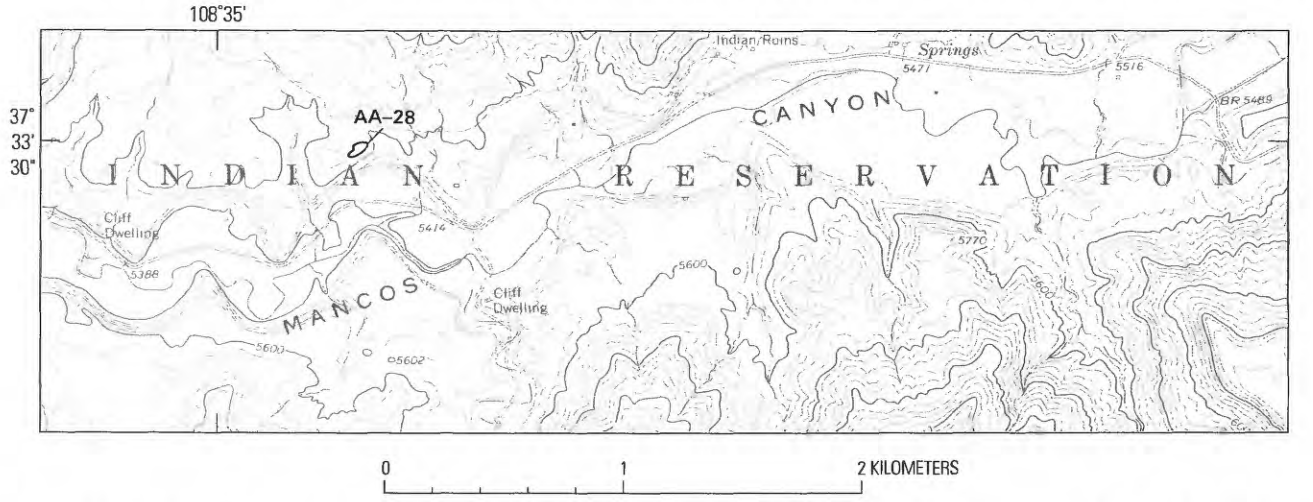

Figure 13. Location of heavy-mineral deposit AA–28 in the northern part (Colorado) of the Ute Mountain Ute Indian Reservation. Topographic base from U.S. Geological Survey Moqui Canyon (1966) quadrangle, scale 1:24,000. Contour interval is 40 ft (12.2 m).

GROUND MAGNETOMETER SURVEY

The total magnetic field was measured using a proton-precession magnetometer along five traverses. Traverses 1, 2, and 4 (figs. 14 and 15) crossed exposed deposits, and traverses 3 and 5 (fig. 15) crossed projected trends of the deposits. Line 1 delineates deposit AA–10 with a peak amplitude of about 100 nanoteslas (nT) (fig.16*A*). AA–11 is marked by a more subdued peak of about 30 nT (fig. 16*B*). Line 3 was about 2,010 m northwest of AA–10 and 1,100 m southeast of AA–17. The magnetic profile (fig. 16*C*), which covers about 1,370 m, lacks obvious magnetic anomalies but displays numerous minor features that have wavelengths of about 15 m and amplitudes of about 5–10 nT. Line 4, across the exposed part of AA–17, reveals a peak of about 75 nT (fig. 16*D*). Line 5, about 520 m southeast of line 4, did not detect deposit AA–17 (fig.16*E*). The only magnetic feature detected is probably a pipeline beneath the road that was also detected in the profile of line 4.

The lack of prominent peaks (except for the pipeline) in the profiles of lines 3 and 5 may be attributed to either the absence of buried deposits or to burial at sufficient depth to mask or eliminate magnetic signals at the surface. It is believed that AA–17 pinches out between lines 4 and 5 because geologic evidence, such as bedding attitude or structure that would indicate an abrupt change in depth of the deposit between the two closely spaced lines, is lacking.

Burial depth must be considered as a possible cause of the subdued magnetic field along line 3, which is remote from deposit exposures. This possibility was evaluated by determining the effects of different burial depths on the magnetic profile obtained in line 1. Using the upward-continuation method, we generated the magnetic-field profiles (fig. 17) that would have been observed had AA–10 been buried between 3 and 21 m. The analysis yielded the approximate depths to which magnetic detection of deposits of the type in the study area is feasible. For example, at 3-, 9-, and 21-m-separation increments between observer and source, the peak amplitudes decrease from about 100 nT to about 60 nT, 30 nT, and 10 nT, respectively.

This analysis indicates that deposits having magnetizations equivalent to those of AA–10 are undetectable at the surface if buried by more than about 20 m. Considering the elevations of lines 1 and 3, the bedding attitudes, and the lack of known faults in the study area, it is unlikely that AA–10 occurs below line 3 at depths greater than 20 m; more likely, this deposit does not even extend to the vicinity of line 3.

MAGNETIZATION OF HEAVY-MINERAL DEPOSITS

MAGNETIC SUSCEPTIBILITY AND NATURAL REMANENT MAGNETIZATION

Magnitudes of magnetic susceptibility (MS) at the outcrop and magnitudes of natural remanent magnetization (NRM) of samples returned to the laboratory from AA–10 were measured to investigate the variability of these properties in the deposit (table 2). Magnetic susceptibility is a measure of the magnetization induced in rock in the presence of a weak, low-amplitude magnetic field. Natural remanent magnetization is the entire permanent magnetization of a rock. The magnetic properties were found to vary systematically with respect to the geometry of the deposits and they yielded information on postdepositional alteration.

Magnetic susceptibility was measured at the outcrops of AA–10 and AA–17 using a portable susceptometer having a sensitivity of about 5×10^{-5} SI (Systeme Internationale units). At both exposures, MS was relatively low at the margins of the deposits and increased toward the interior. The spatial change of MS is illustrated in a schematic cross section of

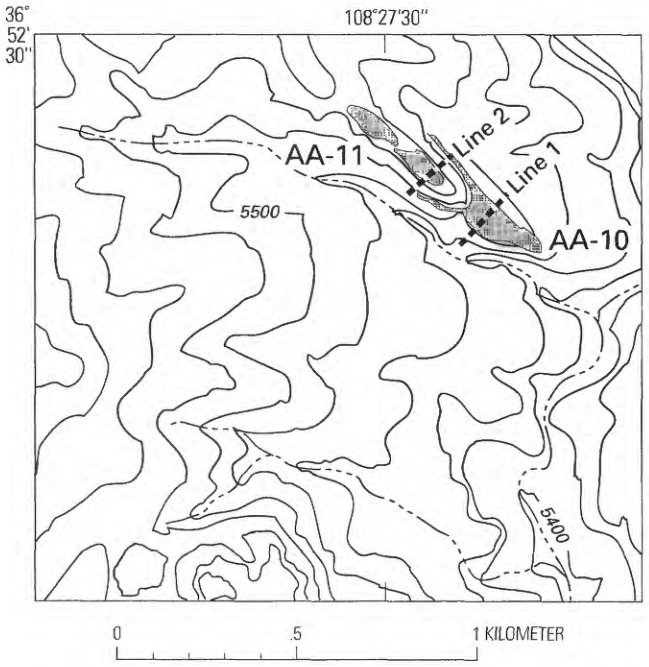

Figure 14. Ground magnetometer survey traverse lines 1 and 2 across anomalies AA–10 and AA–11. Topographic base from U.S. Geological Survey Waterflow (New Mexico) quadrangle, scale 1:24,000. Contour interval is 40 ft (12.2 m).

AA–10 with contoured MS values, shown in figure 18. Laboratory measurement of MS and NRM of samples from AA–17 bear out the observations made at the outcrop and indicate that the NRM magnitude, which commonly mimics variations in MS, is also highest in the center of the deposit (table 2; fig. 19).

The high MS and NRM in the centers of the heavy-mineral deposits suggests that magnetite is relatively more abundant in the interior parts than at the margins. The variations in magnetic properties correlate with variations in the colors of the deposits in the outcrops. In general, black rocks are characteristic of the interior zones of high magnetization, whereas brown and brown-red hues characterize the margins that have substantially lower magnetization.

PETROLOGIC AND ROCK MAGNETIC INVESTIGATIONS

The causes of variation in magnetization in the deposits were investigated using a combination of petrologic and rock magnetic methods. These methods included reflected-light microscopic examination of polished thin sections and of polished grain mounts of magnetic separates, thermomagnetic analysis, and rock magnetic tests that, for our purposes, allow distinction primarily between hematite and magnetite. In thermomagnetic analysis, magnetic grains are heated and then cooled in the presence of a strong magnetic field, and the resulting changes in magnetization enable mineral identification by defining, for example, the Curie temperatures of the grains. The Curie temperature is the temperature at which a ferrimagnetic substance loses its ferrimagnetism, or spontaneous magnetic ordering. Together, the results and observations from the petrologic and rock magnetic methods enable identification of the minerals responsible for magnetization of the deposits and yield information on their distributions.

Petrographic examination of polished thin sections confirmed the presence of abundant titanium-bearing magnetite in the highly magnetic interior portions of the deposits; magnetite was not observed in samples from the more weakly magnetized margins. Instead, the weakly magnetized rocks contain abundant grains of titaniferous magnetite that has been postdepositionally altered by leaching of iron, leaving relict titanium-rich minerals such as anatase.

The zones of high and low magnetization have different interstitial cements. Calcite cement occurs in the strongly magnetized sandstones that contain magnetite and other detrital oxide minerals that lack obvious or extreme postdepositional alteration. The calcite contains sparse framboids of pyrite that appear to have formed during early diagenesis. In contrast, ferric-oxide phases completely fill interstitial areas in sandstones in which titaniferous magnetite was strongly altered by leaching of iron. Relicts of framboidal pyrite are rarely found within the oxide cement, but there is no evidence of another generation of sulfide minerals that would postdate the pyrite seen in the interior zones of the deposits.

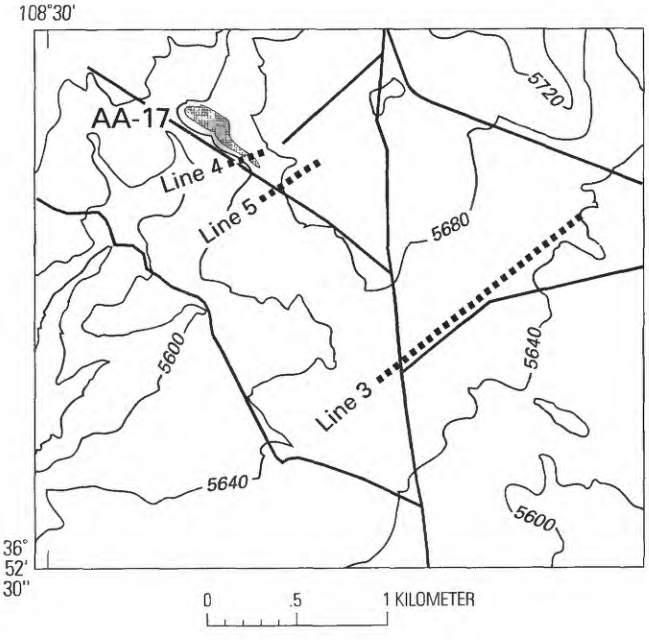

Figure 15. Ground magnetometer survey traverse lines 3, 4, and 5 in the vicinity of anomaly AA–17. Topographic base modified from U.S. Geological Survey Heifer Point (New Mexico) quadrangle, scale 1:24,000. Contour interval is 40 ft (12.2 m).

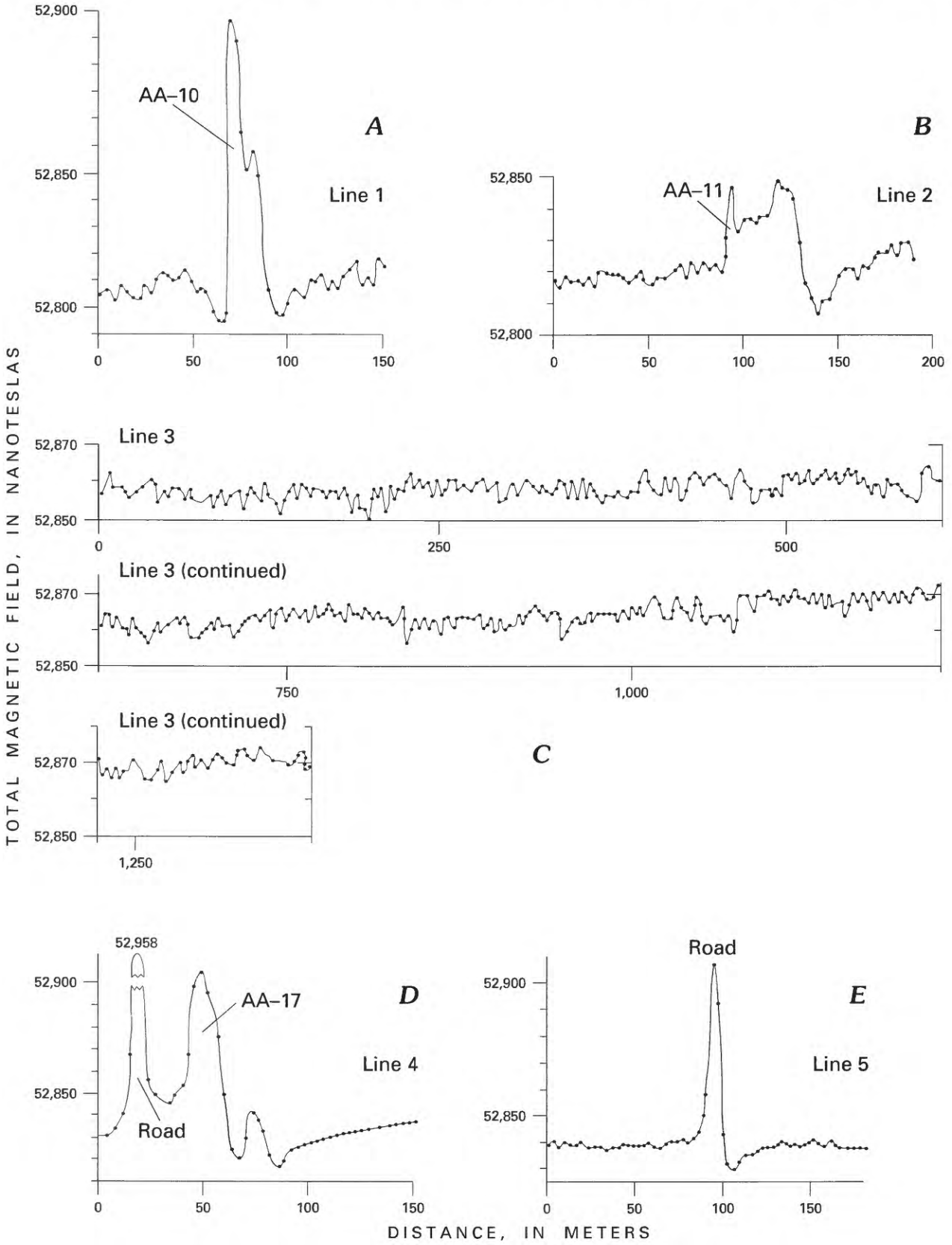

Figure 16. Magnetic profiles from ground magnetometer traverses conducted in the southern group of anomalies (lines shown in figs. 14 and 15). Profiles begin at the southwest end of each line.

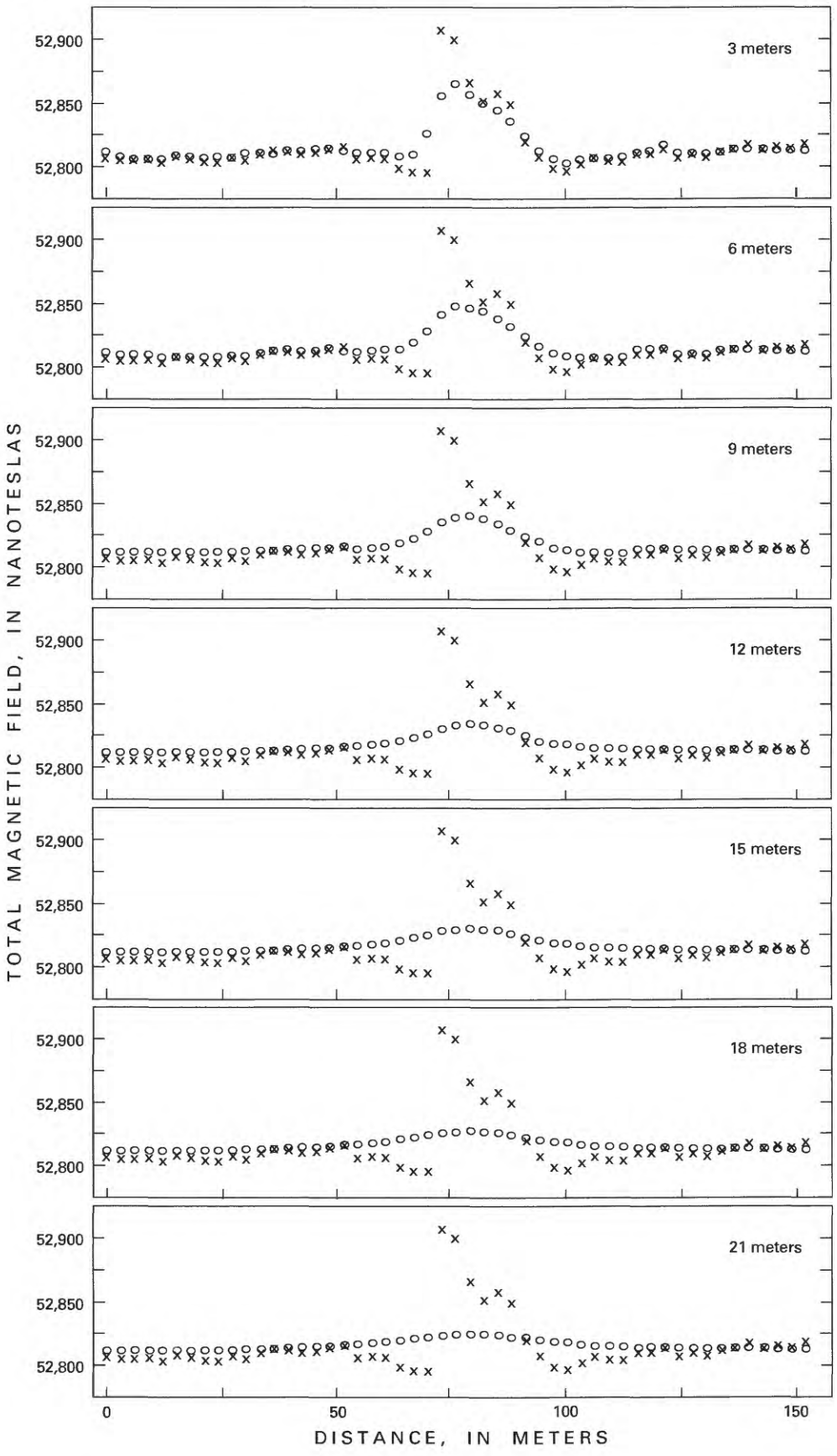

Figure 17. Plots generated using the upward-continuation method in which the magnetic profile obtained from line 1 (fig. 16*A*), shown here with crosses, is plotted against the synthetic profiles (circles) at the various depths indicated.

Table 2. Magnetic properties of samples from AA–17.

[Magnetic sample numbers start with 7UM; corresponding geochemical sample numbers are given in parentheses. M_{NRM}, magnetic dipole moment in SI units of amperes per meter (A/m; 1 A/m=10^{-3} emu/cc); K, magnetic susceptibility in volume SI units (1 vol SI unit of K is equivalent to $1/4\pi$ emu/cc in CGS units); $FeTO_3$, total iron oxide expressed as Fe_2O_3; (--), none detected]

Sample number	Location	M_{NRM} ($\times10^{-2}$ A/m)	K ($\times10^{-3}$)	$FeTO_3$ (percent)	[1]TiO_2 (percent)
7UM–27 (AA–17–5)	White sandstone above deposit	0.3	0.2	5.89	3.98
7UM–26 (AA–17–4)	Upper part of deposit; 1.3 m below 7UM–27	1.7	0.7	14.61	5.71
7UM–25 (AA–17–3)	Interior of deposit; 0.3 m below 7UM–26	100	65	34.91	5.56
[2]7UM–24	Adjacent to 7UM–25	94	60	--	--
7UM–23 (AA–17–1)	Lower in deposit; 0.7 m below 7UM–24	1.7	0.5	15.42	0.45
[2]7UM–22	Lowermost exposure of deposit (base is covered); 0.3 m below 7UM–23	16	0.4	--	--

[1]Data from appendix.
[2]No corresponding geochemical samples.

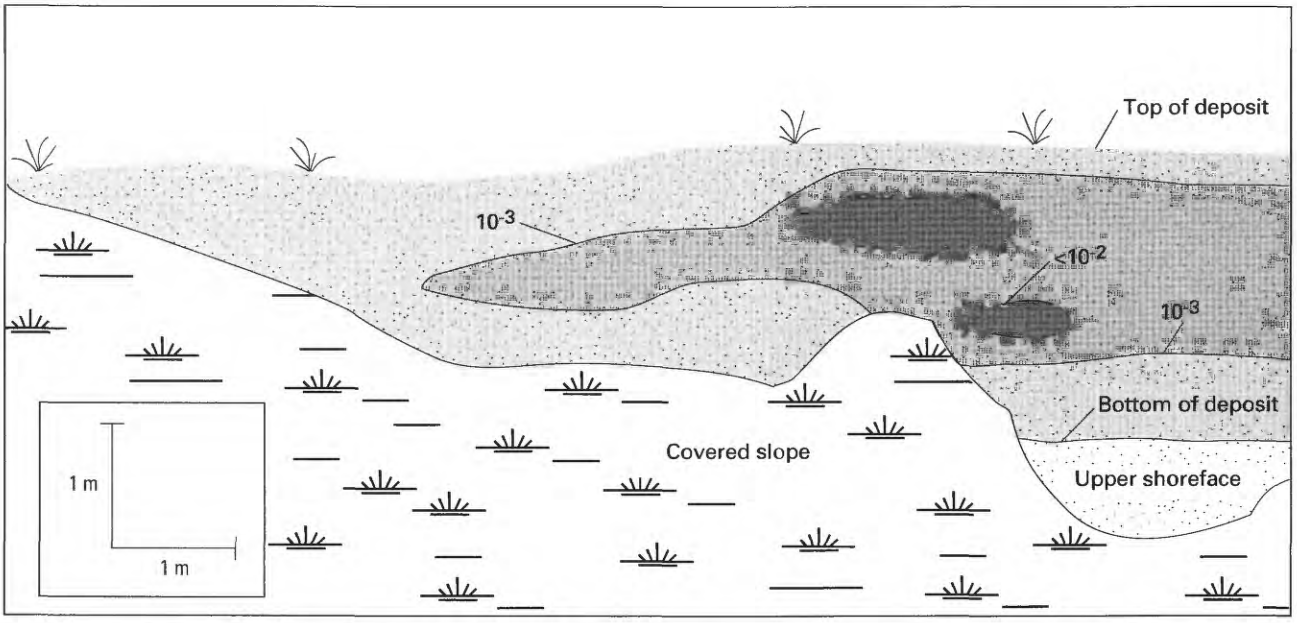

Figure 18. Schematic cross section of deposit AA–10 showing magnetic susceptibility values, in volume SI units (1 volume SI unit is equivalent to $1/4\pi$ electromagnetic units per cubic centimeter in the CGS system), contoured from portable-susceptometer readings taken at the outcrop. Rocks of highest susceptibility occur in the center of the deposit.

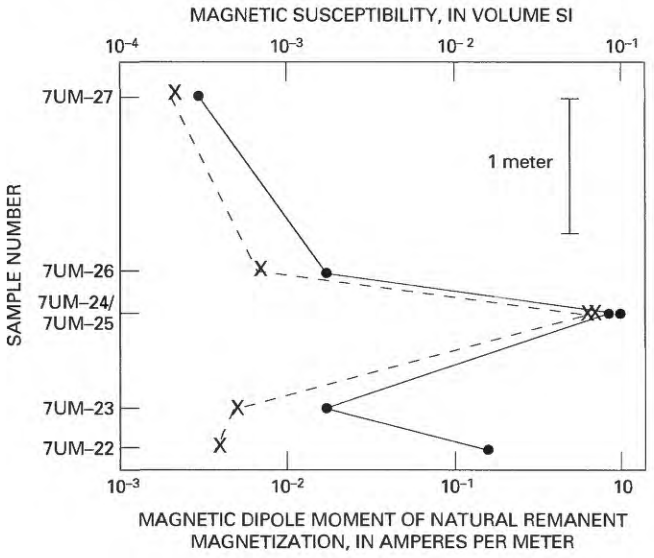

Figure 19. Plot of magnetic properties of samples from deposit at AA–17 showing highest values of magnetic susceptibility (crosses) and magnetic dipole moment of natural remanent magnetization (NRM) (circles) in the center of the deposit. See table 2 for descriptions of the samples.

Detrital iron-titanium oxides other than magnetite are common in the heavy-mineral suite, especially minerals of the ilmenite-hematite series (titanohematites). Over a range of intermediate compositions (20–40 mol percent hematite), the titanohematites are ferrimagnetic (strongly magnetic). A polished grain mount of the magnetic separate from sample AA–10–9 indicates abundant titanohematite that contributes to the magnetization of the deposits.

Thermomagnetic analysis confirms the petrographic identification of titanohematite in sample AA–10–3 (fig. 20). The thermomagnetic curve for AA–10–3 shows an abrupt initial loss of magnetization at the onset of heating and an abrupt gain in magnetization upon cooling below about 250°C. Such behavior is diagnostic for ferrimagnetic titanohematite when considered with the petrographic observations (Reynolds, 1977). The parts of the heating and cooling paths at temperatures above about 300°C and the irreversibility of the curves are difficult to explain. Irreversibility refers to the failure of the cooling curve to trace back on or near the heating curve. Magnetite was absent in the original sample, but apparently it was produced from the sample during heating, as indicated by the minor increase in magnetization from 490 to 510°C. The absence of a sharp increase in magnetization near 580°C, the Curie temperature for magnetite upon cooling, indicates that the magnetite was oxidized to ferric oxide shortly after its formation. The cause of the production of magnetite is not known. Pyrite is present in very minor amounts in the sample, but it is not a precursor of the magnetite because under the experimental conditions of the instrument, pyrite converts to magnetite at temperatures near 350°C. The abundant interstitial ferric-oxide cement in this sample probably is responsible for the magnetization above 580°C.

The thermomagnetic curve for AA–17–3 (fig. 20), a sample known to contain abundant magnetite, is irreversible and shows a remarkably abrupt and unusual increase in magnetization at 490°C that resulted from the production of an additional large quantity of magnetite. In this case, the magnetite was preserved and perhaps continued to grow despite continued heating to 620°C, as indicated by the strong gain in magnetization upon cooling below 580°C. Again, oxidation of pyrite to form magnetite cannot account for the formation of additional magnetite. Sample AA–17–3 contains abundant calcite cement and is devoid of ferric-oxide cement. The high-temperature oxidation of other iron-titanium-oxide minerals such as titanomagnetite or titanomaghemite may have generated magnetite during the experiments.

Other rock magnetic tests were conducted to supplement the petrographic and thermomagnetic analyses. These tests included the alternating-field (AF) demagnetization of NRM, the acquisition of isothermal remanent magnetization (IRM), and the removal of the IRM in a strong magnetic induction field directed opposite to the induction in which the IRM was acquired. These tests yield information on the coercivity (or magnetic "hardness") of the rocks and their magnetic minerals. Coercivity, the opposing applied magnetic field that reduces the remanent magnetization of a substance to zero, varies for different magnetic minerals. The results from these tests elucidate qualitatively the contributions to magnetization from the titanomagnetites and titanohematites, which have relatively low coercivities, and from hematites (and perhaps other ferric oxides), which have higher coercivities. In this study, the results mainly reflect the distribution of detrital titanomagnetite and titanohematite relative to that of the interstitial ferric oxide that occurs antipathetically with magnetite.

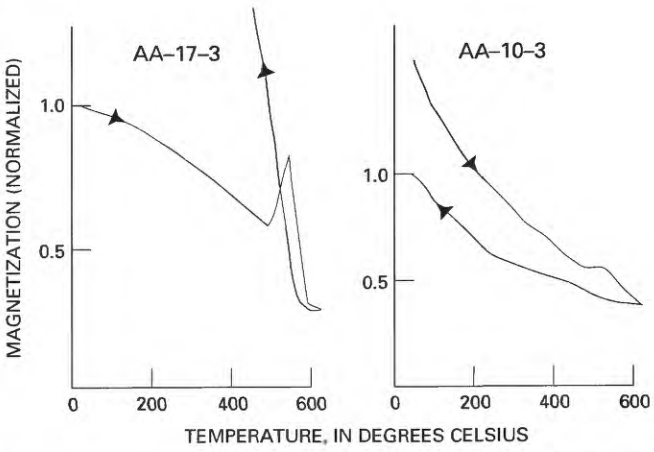

Figure 20. Thermomagnetic curves for samples AA–17–3 and AA–10–3.

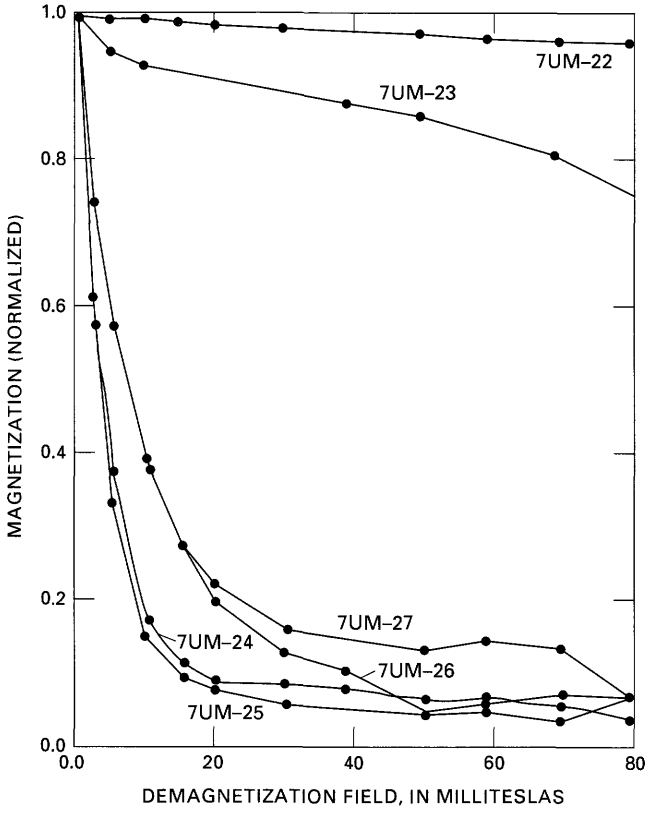

Figure 21. Alternating-field (AF) demagnetization plots of samples from AA–17 showing decay of the magnetic dipole moment of NRM (normalized magnetization) with respect to the demagnetization field.

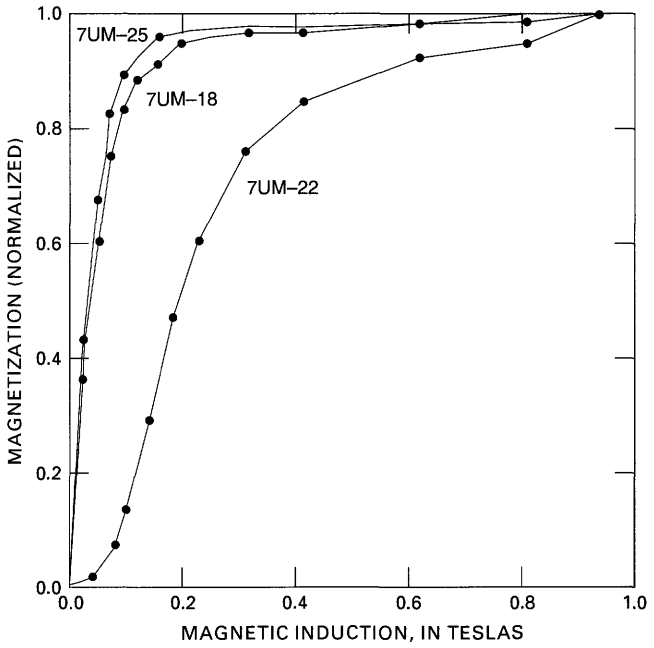

Figure 22. Curves of acquisition of isothermal remanent magnetization (IRM) showing magnetization (normalized) plotted against magnetic induction. Sample 7UM–18 is from AA–10; others are from AA–17.

High coercivities of magnetic minerals are revealed in plots of AF demagnetization by a low decay of NRM magnitude with increase in the demagnetization field, whereas relatively low coercivities are indicated by a substantial decrease in magnetization with higher demagnetization fields (fig. 21). Samples 7UM–22 and 7UM–23, which are from the lower part of AA–17, show the dominantly high coercivity behavior characteristic of hematite. In contrast, samples 7UM–24 and 7UM–25, from the highly magnetized center of the deposit, have low coercivities typical of magnetite-bearing rocks. AF demagnetization curves for samples 7UM–26 (upper part of deposit) and 7UM–27 (above the deposit) lie close to but above those for samples 7UM–24 and 7UM–25. Samples 7UM–26 and 7UM–27 thus appear to contain a combination of magnetite and ferric oxide (even small quantities of magnetite dominate magnetic signals in rocks that contain volumetrically more hematite).

Curves of IRM acquisition (fig. 22) show the distinction between magnetization carried dominantly by magnetite and that carried dominantly by ferric oxide. In IRM acquisition tests, the magnetization is imparted to a sample in the presence of an incrementally increased magnetic induction instead of reduced from the sample as in the AF-demagnetization method. In this procedure, magnetite is more readily magnetized than the magnetically "harder" ferric oxide. Thus, magnetite-bearing rocks acquire a greater portion of their saturation IRM at low inductions relative to hematite-bearing samples. Again, the magnetite-dominant magnetization in sample 7UM–25 contrasts with the ferric-oxide-dominant magnetization in sample 7UM–22 (fig. 22). Sample 7UM–18, shown in figures 22 and 23, is from the magnetite-rich part of AA–10.

Similar information is obtained from examination of curves generated by removing IRM. The magnetic induction at which the IRM is reduced to zero, termed the coercivity of remanence, is sensitive in this application to magnetic mineralogy. IRM of magnetite-bearing rocks is more easily eliminated, giving low negative values of the coercivity of remanence relative to hematite-bearing samples. Curves showing the removal of IRM in figure 23 illustrate the hematite dominance in sample 7UM–22 and the magnetite dominance in samples 7UM–25 and 7UM–18.

Thus, the rock magnetic results show that ferric-oxide minerals dominate the magnetization of samples from the weakly magnetized margins of the deposits, and that magnetite (and perhaps titanohematite—the relative contributions of the two species cannot be discerned in these analyses) dominates the magnetizations of the interiors of the deposits. Therefore, the rock magnetic data corroborate the petrographic observations and results from MS and NRM measurements.

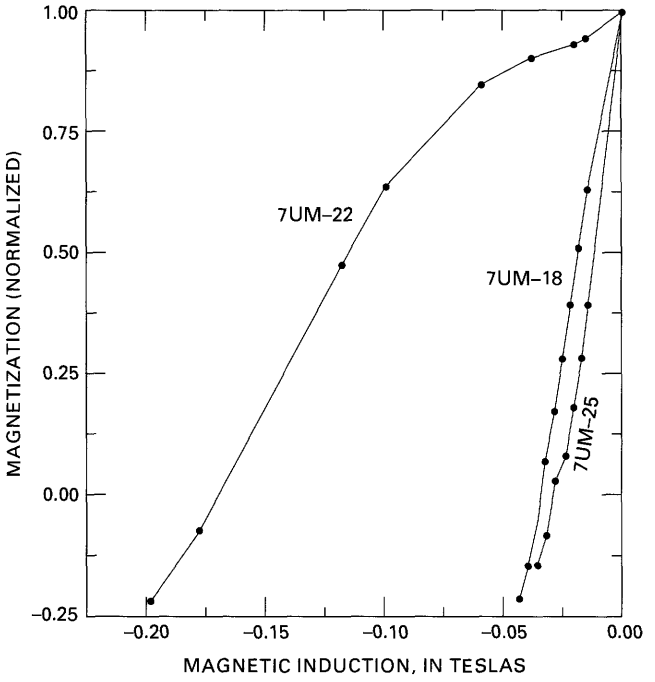

Figure 23. Backfield curves of isothermal remanent magnetization (IRM) showing magnetization (normalized) plotted against magnetic induction. Negative induction values indicate application of the induction in a direction opposite to that applied for acquisition of the IRM. Sample 7UM–18 is from AA–10; others are from AA–17.

GEOCHEMICAL STUDIES

One or two 0.5–1.5 kg grab samples were taken from each deposit except for AA–10 and AA–17, which were sampled more thoroughly because their outcrops facilitated the collection of a vertical series of samples. A total of 51 samples were collected. The intent was to sample an area that would best represent the deposit; however, several characteristics of these deposits made this quite difficult. First, many have limited outcrops with only the upper(?) part exposed above the surrounding Holocene colluvium or eolian sand. In such areas, the relation of the outcrop to the rest of the deposit is unknown. Second, the high degree of induration made sampling difficult. Commonly, only sites of intense fracturing and weathering or areas of less induration were available for sampling. Because of this, many of the samples are from the tops of the deposits or nearby. Third, visual and radiometric observations indicated that the heavy-mineral content of a deposit varied from one horizon to another. This is supported by the findings of the magnetic part of our study and by the multiple samples of AA–10 (see appendix). A deposit may contain relatively barren beds that may be mistaken as heavy-mineral accumulations because of the degree of diagenetic iron cement present (such as in AA–11 and FA–1). Thus, no single sample represents an entire deposit. Each group of samples should be viewed as broadly characterizing the deposit as a whole. A specific analysis can provide insight to the unique characteristics of particular deposits, such as the high zirconium and titanium content of AA–26. Although relatively large samples were collected, an economic evaluation would require larger samples taken systematically through each occurrence.

Each field sample was cut with a rock saw for thin sections and whole-rock specimens. A split of the remaining sample was pulverized with a ceramic shatterbox laboratory mill to –200 mesh for analysis. Pulverized samples were split using a mechanical splitter; one split was for instrumental neutron-activation analysis (INAA) and the other was pressed into pellets for energy-dispersive x-ray fluorescence spectroscopy (XRF) analysis.

CHEMICAL ANALYSES

Results of chemical analyses are shown in the appendix. XRF analysis was used to identify the major elements and the trace elements Cu, Ga, Nb, Pb, and Y. INAA analyzed the remaining trace elements. The major elements are given in percent oxide. INAA trace-element results are reported in alphabetical order in parts per million. The results of the XRF and INAA analyses are from whole-rock samples, reported as received and are not rounded to significant numbers.

ENERGY-DISPERSIVE X-RAY FLUORESCENCE (XRF)

XRF analysis uses two sources to irradiate the samples. Rhodium radiation was used to analyze for major oxides, and ^{109}Cd was used to obtain semiquantitative values for the trace elements Cu, Ga, Nb, Pb, and Y. Johnson and King (1987) summarize the method:

> X-ray fluorescence analysis entails the excitation of X-rays within a sample and their subsequent detection and measurement. * * * During sample irradiation, inner shell electrons of the elements in the sample absorb specific X-ray photons and are ejected from the atom. Rearrangement of the remaining electrons to fill these vacancies causes the emission of so-called fluorescent X-rays, whose energies are characteristic of the elements from which they originate. * * * X-rays emitted by the sample are absorbed in the detector, which acts as a diode in converting these incident X-rays to electronic pulses whose amplitudes are proportional to the energies of the corresponding X-rays. Pulses then are processed and sorted according to amplitude: * * * The intensity, or number of counts in a peak, is a direct result of the number of fluorescing atoms of that element in the sample; thus, the area under a peak is proportional to the concentration of that element in the sample.

INSTRUMENTAL NEUTRON-ACTIVATION ANALYSIS (INAA)

The INAA technique is well summarized by Baedecker and McKowen (1987):

Instrumental activation analysis with thermal neutrons (INAA) is a versatile technique for elemental analysis because it has a high sensitivity for many elements, * * * and provides precise data for many major, minor, and trace elements in a single sample aliquant without chemical treatment. * * * The method is based on the irradiation of samples and standards in a reactor neutron flux and the measurement of the induced radioactivity using high resolution gamma-ray spectrometry. The technique has a sensitivity ranging from 0.1 to 10 parts per million for a wide range of elements including many of the first row transition elements, rare earths, alkali, and alkaline earths.

ANALYTICAL CONSIDERATIONS

In XRF analysis, sample composition and preparation, relative elemental concentrations, and major concentrations of an element (such as iron) affect the analytical results. The most conspicuous effect is that the total of major oxides in the samples is considerably less than 100 percent. The reasons for this are discussed in the following paragraphs. Although the lower oxide values are noteworthy, titanium, which is the most important economic element in the oxides, is relatively unaffected.

The lower oxide values of the deposit samples are caused by several factors. One cause is the trace elements, which may exceed 6 percent of the sample. Another is the XRF method, which does not account for the large mass-absorption contributions of Na, Mg, and Fe and the mineralogic effects due to differences in standards and samples. This is particularly important as the Fe content increases in the samples. A third cause is the mineralogic effect that significantly reduces the SiO_2 values in the oxide analysis. This was confirmed by XRF analysis on selected fused duplicate samples. The analysis showed an SiO_2 value that was consistently 10 percent lower in the packed-powder samples (other oxide values remained fairly constant). And fourth, XRF is incapable of analyzing all of the major elements, in particular carbon (in CO_2 and organic carbon) and hydrogen (in H_2O+). This results in lower oxide totals because: (1) CO_2 contained in carbonates including calcite ($CaCO_3$), siderite ($FeCO_3$), ankerite [$Ca(Fe,Mg,Mn,)(CO_3)$], and dolomite [$CaMg(CO_3)_2$] will not be detected; and (2) structural water is not detected, and deposit samples have some clay and higher quantities of mica compared to the barren samples. Loss on ignition, which quantifies the volatile fraction, ranged from 6.1 to 14.7 percent on six random samples.

In the INAA method, composition, preparation, and relative elemental concentrations affect the detection limits because of elemental sparsity and overlap of detection peaks. Major concentrations of an element such as iron have an effect on the detection limits and accuracy. It is believed that samples with relatively high levels of iron (>5 percent) give analyses with higher detection limits and lower accuracy for some elements. This interference, however, will not affect discrimination between the elements. In general, the values for the elements in high-iron samples are expected to have a precision of ±20 percent. Because the purpose of the analysis is to indicate potentially economic elemental abundance, errors in the detection level are not significant, and precision errors of as much as 20 percent will still show concentration trends of interest.

DISCUSSION OF SELECTED ELEMENTS

The elements considered in this section (Fe, Ti, Zr, U, Th, Y, Cr, Au, and rare-earth elements) were selected because of their economic potential. However, the appendix includes all the analyzed elements because they may have value in understanding the chemistry or mineralogy of the deposit and may have some importance in future evaluations.

Table 3 shows the oxide and trace-element average compositions for barren samples (AA–10–1, AA–10–2, AA–10–3, AA–10–5, and AA–17–1) and mineralized samples. All barren rock samples were determined by field criteria and confirmed by analytical results. Anomalies AA–11 and FA–1 were identified in the field as heavy-mineral deposits, but analyses later showed that their samples were from iron-cemented but relatively barren beds within the deposits. These samples were not included in the average values shown in table 3.

IRON

Except for SiO_2, iron oxide is the dominant compound in the deposits, ranging from 0.7 to 35 percent of the whole rock. The presence of large amounts of iron has a substantial negative impact on the economics of a heavy-mineral deposit because it introduces additional costs to mining, disaggregation, and milling. The iron occurs mostly as a ferric-oxide cement. This degree of iron cementation is unusual in Holocene heavy-mineral deposits even though it is common in fossil deposits (Wedow and Hobbs, 1968; Dow and Batty, 1961). Although some of the induration is due to calcite cement and part of the characteristic color is due to manganese, the iron content of the rock is mostly responsible for these qualities. The dark color is a primary field guide because it is always present in areas of maximum heavy-mineral concentrations. However, it is not always present in areas of moderate concentrations. As an example, sample AA–10–6 (see appendix) was collected from a light-colored bed but has a relatively high Zr value (4,200 ppm) and TiO_2 value (4.34 percent). A scintillometer is a useful reconnaissance tool in such situations because it detects the radioactivity associated with the heavy-mineral concentrations.

Petrographic observations suggest reducing conditions of alteration under which iron was leached from titaniferous magnetite and ilmenite, leaving relict grains rich in titanium dioxide. Iron was subsequently redeposited as ferric-oxide phases in interstitial areas between the detrital heavy minerals. Leaching of iron may have been facilitated (by complexing, for instance) with organic acids derived from the overlying Menefee Formation. For additional information on the Eh/pH behavior of iron and iron solubility, see Garrels and Christ, (1965, fig. 7.11).

TITANIUM

Titanium (in the form of TiO_2) is the primary economic element in many modern heavy-mineral placers. On the Reservation, TiO_2 ranges from about 0.4 to 21 percent and averages 7.9 percent. Titanium is contained in ilmenite, titanomagnetite, titanohematites, and small amounts of titanium-oxide minerals including rutile, anatase, and brookite. The relative abundance of these minerals varies depending on the deposit, degree of iron alteration, and the location of the sample (see section on petrology and rock magnetic investigations).

TiO_2 may constitute as much as one-fifth of a lithified heavy-mineral deposit (Wedow and Hobbs, 1968). The TiO_2 content is greater in older deposits, primarily because of increased leaching of iron from ilmenite and the alteration of ilmenite to leucoxene (U.S. Bureau of Mines, 1985; Staatz and others, 1980). Some of the heavy-mineral deposits in the San Juan basin average 16 percent TiO_2, with a maximum of 32 percent (Chenoweth, 1957). In the same article, Chenoweth reported a 21.5 percent TiO_2 value from a Ute Mountain Ute Indian Reservation sample (probably from AA–17 or AA–18).

One unusual titanium occurrence (4.51 percent TiO_2) on the Reservation is in a sandy mudstone in AA–10, about 19.8 m above the base of the section (fig. 10). This mudstone lies on a ravinement surface where sediments were transgressed and eroded (see description of airborne anomaly AA–10 in the discussion of the southern anomaly group). The mudstone is part of a minor transgressive event and contains some of the heavy minerals from the eroded and reworked underlying foreshore sediments. The areal extent and patterns of heavy-mineral concentrations in these transgressive mudstones are unknown. Future investigations of heavy-mineral deposits should include this facies.

ZIRCONIUM

Zirconium, from the mineral zircon, may be the second most valuable element in these deposits. Zircon has risen in value and in many mines is considered a coproduct instead

Table 3. Average compositions of oxides and trace elements from semiquantitative analyses of the barren and heavy-mineral samples from the Ute Mountain Ute Indian Reservation.

Substance	Barren samples[1]	Mineralized samples[2]
	Oxides (percent)	
SiO_2	81.76	38.80
Al_2O_3	10.09	4.16
[3]$FeTO_3$	4.46	18.75
MnO	0.05	0.51
MgO	0.36	0.68
CaO	0.48	5.38
Na_2O	1.70	0.40
K_2O	1.84	0.25
TiO_2	0.46	7.93
P_2O_5	0.09	0.34
SO_3	0.03	0.29
Total	101.32	77.49
	Trace elements (parts per million)	
Ag	1	3.80
As	3.34	4.70
Au	0.09	0.03
Ba	544	411.62
Br	1.32	2.24
Ce	50.6	1,157.65
Co	8.2	49.28
Cr	96	856.76
Cs	1.54	0.71
Cu	47.2	99.81
Eu	0.5	3.11
Ga	11.8	54.08
Hf	3.8	340.05
La	30	740.54
Lu	0.32	6.84
Mo	0.6	1.32
Nb	6.2	172.73
Ni	10	28.14
Pb	12.6	97.11
Rb	55.8	13.45
Sb	0.74	1.59
Sc	7.28	49.16
Se	2.5	3.96
Sm	3.98	85.03
Sr	64.6	39.00
Ta	0.34	14.27
Tb	0.53	8.60
Th	7.64	278.11
U	1.99	46.57
W	0.9	13.77
Yb	1.8	38.70
Y	14.8	255.73
Zn	50	236.62
Zr	224	14,490.00

[1]Samples AA–10–1, AA–10–2, AA–10–3, AA–10–5 and AA–17–1.
[2]All samples except barren samples and those from FA–1 and AA–11.
[3]Total iron oxide expressed as Fe_2O_3.

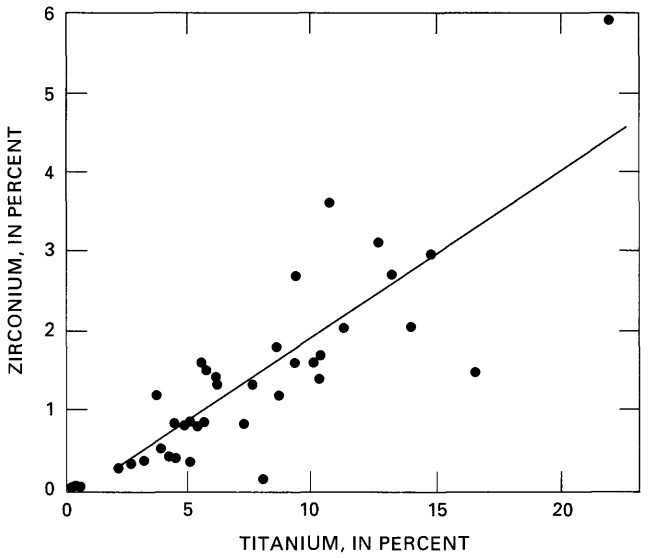

Figure 24. Plot of zirconium versus titanium content in heavy-mineral samples analyzed. Line represents a linear best-fit curve to the data.

of a byproduct. The average zirconium content in deposit samples is 1.4 percent. A sample from AA–26 contained almost 6 percent zirconium, the highest amount found in any of the deposits on the Reservation. By comparison, Wedow and Hobbs (1968) have reported zircon values in other lithified titanium-rich heavy-mineral deposits in the United States ranging from 5.5 to 9 percent (2.6–4.4 percent zirconium).

In general, the amounts of titanium and zirconium in Reservation deposits increase and decrease together in a ratio of about 5:1 (see appendix). This is shown by plotting titanium versus zirconium content in Reservation samples (fig. 24).

RARE-EARTH ELEMENTS

Rare-earth elements (REE) is a collective term for 15 elements with atomic numbers from 57 to 71 (the lanthanides). Yttrium, scandium, and thorium (atomic numbers 39, 21, and 90, respectively) are commonly included with the REE because they have similar chemical properties and generally occur with the other REE.

Most REE are obtained from monazite, which is a byproduct of heavy-mineral mining for titanium and zirconium. Monazite is a rare-earth phosphate that commonly contains 50–60 percent rare-earth oxides and 2 percent yttrium oxide (U.S. Bureau of Mines, 1989). Monazite has a wide range of compositions because of appreciable REE substitutions. Its chemical formula is commonly shown as (Ce, La, Y, Th) PO_4, but it may contain varying amounts of other REE. Monazite was identified in several samples from the Reservation by its characteristic fluorescence under a mercury vapor lamp, x-ray diffraction techniques, and energy-dispersive fluorescence using a scanning-electron microscope. Using oxide and trace-element averages (table 3), the monazite content of mineralized samples was calculated and found to constitute as much as 0.2 weight percent. Other heavy minerals that can contain REE include apatite, zircon, sphene, and epidote.

URANIUM AND THORIUM

The average uranium and thorium values (46.57 ppm and 278.11 ppm, table 3) are relatively low. Most of the uranium and some of the thorium in the deposits probably reside in zircon, where they are minor constituents. Zircon is generally used without separation of the uranium and thorium, which are tolerated but not desired components in commercial applications. Uranium may also be present in monazite, and some uranium may be absorbed by ferric oxides.

Most of the thorium probably occurs in monazite, which may contain as much as 12 percent thorium (Deer and others, 1966). Thorium is produced as a byproduct in monazite processing. Thorium in monazite and uranium and thorium in zircon are responsible for the characteristic radioactivity of heavy-mineral deposits.

OTHER ELEMENTS

Yttrium is found in xenotime (YPO_4) and in monazite. Because xenotime was not found in the Reservation samples, the yttrium probably occurs in the monazite. Yttrium is a low-volume but high-value commodity. Except for AA–26–SE, the yttrium values are relatively low.

Chromium is found in fairly high quantities for whole rock. It may be in ilmenite, or it may be complexed with some of the other oxides in the deposits. Chromium is important because it may negatively affect the marketability of ilmenite or adversely affect the milling of other elements (Grosz, 1987).

Gold is present in very small amounts in most samples. The average gold content is 0.09 ppm in barren samples and 0.03 ppm in mineralized samples (table 3). The higher barren-sample value is probably due to the sparsity of gold in the samples, the small sample size, and the relatively few barren samples. Larger samples are required for economic evaluation. Depending on the mineralogic occurrence, gold may or may not be economically important.

Zinc, like gold, is found in small quantities in many samples. Zinc may occur in magnetite and other ferromagnetic minerals in the heavy-mineral deposit. Zinc is a noneconomic element in these deposits and is of interest only if it occurs as gahnite, a zinc spinel that is difficult to separate from rutile.

CONCLUSIONS

Measured sections and stratigraphic observations at each anomaly site on the Reservation show that virtually all the heavy-mineral deposits are at the top of the Point Lookout Sandstone. Sedimentary structures and adjacent sedimentary environments indicate that the heavy-mineral deposits are in foreshore (beach) facies. The alignment of the deposits (fig. 2) defines a linear shoreline system oriented N. 55°– 60° W. that allows extrapolation of the trend to the northwest, where little is known about the deposition of equivalent rocks. This alignment and depositional setting gives the deposits a predictable shape and trend and allows speculation about their subsurface extent.

If there is any subsurface extension from the northern heavy-mineral group, it would lie between airborne anomalies AA–38 and AA–28, an area of significant overburden. In the central group, only anomaly AA–26 has the possibility of subsurface extension. In the southern group, subsurface extensions are possible between airborne anomalies AA–13 and AA–21 and between AA–8 and AA–17, but the potential for a subsurface heavy-mineral deposit between AA–8 and AA–17 is limited by negative magnetization results.

The magnetic portion of this study indicates that such surveys are potentially useful tools for locating heavy-mineral deposits that are buried by less than 20 m of overburden. The magnetization is provided mainly by detrital titaniferous magnetite concentrated in the centers of the deposits. Magnetite was apparently deposited relatively evenly throughout the deposits, but postdepositional alteration destroyed large quantities of the magnetite near the margins. Iron cementation may be the result of humic acids migrating from organic material in the overlying Menefee Formation. Such acids may have mobilized iron from minerals, especially titaniferous magnetite, in the section. Ferric oxide was then deposited interstitially in the deposit.

The heavy-mineral deposits on the Reservation are of economic importance because of, primarily, their relatively high titanium and zirconium content and, secondarily, their various REE byproducts. Semiquantitative analysis showed that titanium content averages 7.9 percent and may reach as much as 21 percent in the whole-rock samples. Zirconium averages 1.5 percent and can make up as much as 6 percent of the whole rock. However, the limited volume of the individual deposits, high iron content, degree of cementation, and distance to water, mills, and markets are factors that negatively affect the economic potential of heavy-mineral deposits on the Reservation.

REFERENCES

Allen, J.E., and Balk, Robert, 1954, Mineral resources of Fort Defiance and Tohatchi quadrangles, Arizona and New Mexico: [New Mexico] State Bureau of Mines and Mineral Resources Bulletin 36, 192 p.

Aubrey, W.M., 1991, Geologic framework of Cretaceous and Tertiary rocks in the Southern Ute Indian Reservation and adjacent areas in the northern San Juan basin, southwestern Colorado, chap. B *of* Zech, R.S., ed., Geology and mineral resources of the Southern Ute Indian Reservation: U.S. Geological Survey Professional Paper 1505–B, 24 p.

Baedecker, P.A., and McKowen, D.M., 1987, Instrumental neutron activation analysis of geochemical samples, *in* Baedecker, P.A., ed., Methods for geochemical analysis: U.S. Geological Survey Bulletin 1770, p. H1–H14.

Bingler, E.C., 1963, Niobium-bearing Sanostee heavy-mineral deposit, San Juan basin, northwestern New Mexico: New Mexico Bureau of Mines and Mineral Resources Circular 69, 63 p.

Blagbrough, J.W., 1955a, San Juan basin airborne anomaly No. 6, Ute Mountain Indian Reservation, San Juan County, New Mexico: U.S. Department of the Interior, U.S. Geological Survey Trace Elements Preliminary Reconnaissance Report ED–R–450, 2 p.

———1955b, San Juan basin airborne anomaly No. 5, Ute Mountain Indian Reservation, San Juan County, New Mexico: U.S. Department of the Interior, U.S. Geological Survey Trace Elements Preliminary Reconnaissance Report ED–R–449, 2 p.

Chenoweth, W.L., 1955a, Northwest San Juan basin airborne anomaly #6, Ute Mountain Indian Reservation, San Juan County, New Mexico: U.S. Department of the Interior, U.S. Geological Survey Trace Elements Preliminary Reconnaissance Report ED–R–445, 2 p.

———1955b, Northwest San Juan basin airborne anomaly #7, Ute Mountain Indian Reservation, San Juan County, New Mexico: U.S. Department of the Interior, U.S. Geological Survey Trace Elements Preliminary Reconnaissance Report ED–R–435, 2 p.

———1955c, Northwest San Juan basin airborne anomaly Nos. 8 and 9, Ute Mountain Indian Reservation, San Juan County, New Mexico: U.S. Department of the Interior, U.S. Geological Survey Trace Elements Preliminary Reconnaissance Report ED–R–433, 2 p.

———1955d, Northwest San Juan basin airborne anomaly Nos. 10 and 11, Ute Mountain Indian Reservation, San Juan County, New Mexico: U.S. Department of the Interior, U.S. Geological Survey Trace Elements Preliminary Reconnaissance Report ED–R–434, 2 p.

———1955e, Northwest San Juan basin airborne anomaly No. 29, Ute Mountain Indian Reservation, Montezuma County, Colorado: U.S. Department of the Interior, U.S. Geological Survey Trace Elements Preliminary Reconnaissance Report ED–R–467, 2 p.

———1955f, Northwest San Juan basin airborne anomaly No. 45, Ute Mountain Indian Reservation, Montezuma County, Colorado: U.S. Department of the Interior, U.S. Geological Survey

Trace Elements Preliminary Reconnaissance Report ED–R–500, 2 p.

———1955g, Northwest San Juan Basin, anomalous area near airborne anomaly #21, Ute Mountain Indian Reservation, San Juan County, New Mexico: U.S. Department of the Interior, U.S. Geological Survey Trace Elements Preliminary Reconnaissance Report ED–R–473, 2 p.

Chenoweth, W.L., 1957, Radioactive titaniferous heavy-mineral deposits in the San Juan basin, New Mexico and Colorado, *in* Guidebook of southwestern San Juan Mountains, Colorado: Durango, Colo., New Mexico Geological Society, 8th field conference, September 5–7, 1957, p. 212–217.

Chenoweth, W.L., and Carithers, Ward, 1955, Northwest San Juan basin airborne anomaly #4, Ute Mountain Indian Reservation, San Juan County, New Mexico: U.S. Department of the Interior, U.S. Geological Survey Trace Elements Preliminary Reconnaissance Report ED–R–431, 2 p.

Condon, S.M., 1992, Geologic framework of pre-Cretaceous rocks in the Southern Ute Indian Reservation and adjacent areas, southwestern Colorado and northwestern New Mexico, chap. A *of* Zech, R.S., ed., Geology and mineral resources of the Southern Ute Indian Reservation: U.S. Geological Survey Professional Paper 1505–A, 56 p.

Cumella, S.P., 1983, Relation of Upper Cretaceous regressive sandstone units of the San Juan basin to source area tectonics, *in* Reynolds, M.W., and Dolly, E.D., eds., Mesozoic paleogeography of the west-central United States: Denver, Colo., Society of Economic Paleontologists and Mineralogists, Rocky Mountain Section, p. 189–199.

Deer, W.A., Howie, R.A., and Zussman, J., 1966, An introduction to the rock-forming minerals (8th ed.): London, Longmans, Green and Co. Ltd., 528 p.

Devine, P.E., 1991, Transgressive origin of channeled estuarine deposits in the Point Lookout Sandstone, northwestern New Mexico—A model for Upper Cretaceous, cyclic regressive parasequences of the U. S. Western Interior: American Association of Petroleum Geologists Bulletin, v. 75, p. 1039–1063.

Dow, V.T., and Batty, J.V., 1961, Reconnaissance of titaniferous sandstone deposits of Utah, Wyoming, New Mexico, and Colorado: U.S. Bureau of Mines Report of Investigations 5860, 52 p.

Garrels, R.M., and Christ, C.L., 1965, Solutions, minerals, and equilibria: New York, Harper and Row, 450 p.

Grosz, A.E., 1987, Nature and distribution of potential heavy-mineral resources offshore of the Atlantic coast of the United States: Marine Mining, v. 6, p. 387–394.

Grosz, A.E., Muller, F.L., Uptgrove, Jane, Farnsworth, John, Bell, Christy, Maharaj, S.V., Muessing, Karl, and Hathaway, J.C., 1989, Textural, physiographic, bathymetric, and geologic factors controlling economic heavy minerals distribution in surficial sediments on the Atlantic continental shelf offshore of New Jersey: U.S. Geological Survey Open-File Report 89–683, 32 p.

Hollenshead, C.T., and Pritchard, R.L., 1961, Geometry of producing Mesaverde sandstone of the San Juan basin, *in* Geometry of sandstone bodies, Association of Petroleum Geologists, 45th annual meeting, April 25–28, 1960: Atlantic City, N.J., American Association of Petroleum Geologists Symposium Volume (1961), p. 98–118.

Houston, R.S., and Murphy, J.F., 1977, Depositional environment of Upper Cretaceous black sandstones of the Western Interior: U.S. Geological Survey Professional Paper 994–A, p. A1–A29.

Johnson, R.G., and King, B.-S.L., 1987, Energy-dispersive X-ray fluorescence spectrometry, *in* Baedecker, P.A., ed., Methods for geochemical analysis: U.S. Geological Survey Bulletin 1770–F, p. F1–F5.

Mackie, William, 1923, The principles that regulate the distribution of particles of heavy minerals in sedimentary rocks, as illustrated by sandstones of the north-east of Scotland: Edinburgh Geological Society Transactions, v. 11, p. 138–164.

Mahdavi, Azizeh, 1964, The thorium, uranium, and potassium contents of Atlantic and Gulf Coast beach sands, *in* Adams, J.A.S., and Lowder, W.M., eds., The natural radiation environment: Chicago, University of Chicago Press, p. 87–114.

Murphy, J.F., 1956, U.S. Department of the Interior, U.S. Geological Survey trace elements preliminary report on titanium-bearing sandstone in the San Juan basin and adjacent areas in Arizona, Colorado, and New Mexico: U.S. Geological Survey Open-File Report , 8 p.

Newman, K.L., 1982, Stratigraphic framework of Upper Cretaceous (Campanian) coal in western Colorado: Grand Junction Geological Society, Southeastern Piceance Basin Guidebook, 97 p.

Reynolds, R.L., 1977, Magnetic titanohematite in uranium-bearing sandstones: U.S. Geological Survey Open-File Report 77–355, 21 p.

Rittenhouse, Gorden, 1943, Transportation and deposition of heavy minerals: Geological Society of America Bulletin, v. 54, p. 1725–1780.

Rubey, W.W., 1933, The size distribution of heavy-minerals within a water-laid sandstone: Journal of Sedimentary Petrology, v. 3, p. 256–282.

Staatz, M.H., Hall, R.B., Macke, D.L., Armbrustmacher, T.J., and Brownfield, I.K., 1980, Thorium resources of selected regions in the United States: U.S. Geological Survey Circular 824, 6 p.

Stapor, F.W., Jr., 1973, Heavy-mineral concentrating processes and density/shape/size equilibria in the marine and coastal dune sands of the Apalachicola, Florida, region: Journal of Sedimentary Petrology, v. 43. p. 396–407.

U.S. Bureau of Mines, 1985, Titanium, *in* Mineral facts and problems: U.S. Bureau of Mines Bulletin 675, p. 859–880.

———1989, Metals and minerals, Volume 1 *of* Minerals yearbook (1987): Washington, D.C., U.S. Government Printing Office, 990 p.

Van Wagoner, J.C., Posamentier, H.W., Mitchum, R.M., Jr., Vail, P.R., Sarg, J.F., Loutit, T.S., and Hardenbol, J., 1988, An overview of the fundamentals of sequence stratigraphy and key definitions, *in* Wilgus, C.K., Hastings, B.S., Kendall, C.G.St.C., Posamentier, H.W., Ross, C.A., and Van Wagoner, J.C., eds., Sea-level changes—An integrated approach: Tulsa, Okla., Society of Economic Paleontologists and Mineralogists Special Publication 42, p. 39–45.

Wedow, Helmuth, Jr., and Hobbs, R.G., 1968, Zirconium, *in* Mineral resources of the Appalachian region: U.S. Geological Survey Professional Paper 580, p. 361–364.

Woolsey, J.R., Henery, V.J., and Hunt, J. L., 1975, Backshore heavy-mineral concentration on Sapelo Island, Georgia: Journal of Sedimentary Petrology, v. 45, p. 280–284.

Wright, Robyn, 1986, Cycle stratigraphy as a paleogeographic tool—Point Lookout Sandstone, southeastern San Juan basin, New Mexico: Geological Society of America Bulletin, v. 97, no. 6, p. 661–673.

Wright, Robyn, Katzman, D.K., Montz, M.J., and Zech, R.S., 1989, Coastal and shallow marine cyclicity, *in* Nummedal, Dag, and Remy, R.R. eds, Cretaceous shelf sandstones and shelf depositional sequences, Western Interior basin, Utah, Colorado, and New Mexico: Washington, D.C., International Geologic Congress Field Guidebook, 45 p.

Zech, R.S., 1982, Paleoshorelines in the Upper Cretaceous Point Lookout Sandstone, southern San Juan basin, New Mexico: U.S. Geological Survey Open-File Report 82–135, 23 p.

Zech, R.S., and Wright Dunbar, Robyn, 1989, The Durango delta—Complications on a linear strandplain [abs.]: American Association of Petroleum Geologists Bulletin, Abstracts with Programs, v. 73, no. 9, p. 1179–1180.

Zenkovich, V.P., 1967, The formation of mineral deposits in beaches; Processes of coastal development: New York, Interscience Publisher, p. 676–682.

Published in the Central Region, Denver, Colorado
Manuscript approved for publication January 25, 1994
Graphics prepared by Robert Zech and Carol Quesenberry
Photocomposition by Carol Quesenberry
Edited by John Synnefakis

APPENDIX

APPENDIX—Chemical-composition data from neutron activation and x-ray fluorescence analyses of selected

[$FeTO_3$, total iron oxide expressed as Fe_2O_3. Cd, Ir, Sm, and Te not detected. Major oxides analyzed by x-ray fluorescence (XRF); trace (detection limit follows < symbol)]

Sample numbers	AA–8	AA–9	AA–10–1	AA–10–2	AA–10–3	AA–10–4	AA–10–5
			Major oxides (percent)				
SiO_2	16.43	18.44	73.01	96.6	81.6	68.53	93.66
TiO_2	9.36	14.71	0.69	0.37	0.4	4.51	0.41
Al_2O_3	1.37	3.04	15.49	6.4	12.89	11.99	8.3
$FeTO_3$	32.22	18.88	2.27	1.87	1.58	2.75	1.15
MnO	0.8	0.83	0.01	0.05	0.01	0.05	0.01
MgO	0.35	1.04	0.82	0.23	0.45	1.62	0.12
CaO	4.4	9.71	0.49	0.54	0.45	0.98	0.39
Na_2O	0.32	0.28	2.54	1.05	2.39	0.48	1.18
K_2O	0.06	<0.01	2.61	0.9	2.8	0.31	1.44
P_2O_5	0.35	0.67	0.13	0.1	0.07	0.06	0.05
SO_3	0.37	0.07	0.03	0.01	<0.01	3.04	<0.01
Total	66.03	67.66	98.09	108.12	102.64	94.32	106.68
			Trace elements (parts per million)				
Ag	14	<10	<2	<2	<2	<2	<2
As	10	<4.9	3.2	3.4	7.7	4.4	0.7
Au	0.011	0.02	0.02	0.13	0.16	0.036	0.14
Ba	540	690	720	340	740	290	410
Br	3.7	5.1	<2	<2	<2	6.5	<2
Ce	1680	2740	60	43	42	280	47
Co	81	50	8	<5	7	55	<5
Cr	890	1500	91	77	66	400	96
Cs	<1.5	<1.6	2.8	1.2	1.8	3.3	1
Cu	116	283	34	31	59	71	60
Eu	<4	8	<1	<1	<1	<1	<1
Ga	37	144	6	7	16	24	17
Hf	513	727	6	5	2	90	3
La	814	1710	32	25	25	150	28
Lu	7.6	14	0.4	0.2	0.2	2	0.3
Mo	<4	<5	<1	<1	1	4	<1
Nb	147	385	11	6	6	71	5
Ni	96	<45	<20	<20	<20	37	<20
Pb	230	136	8	8	18	33	15
Rb	<25	<27	70	35	76	24	49
Sb	2.5	1.5	1	0.7	1.1	3.1	0.4
Sc	42.4	92.7	9.3	3.7	3.8	24.6	3.6
Se	<13	<14	<5	<5	<5	<5	<5
Sm	121	161	5	3.8	3.2	18	3.6
Sr	56	50	89	36	94	21	54
Ta	14	32	0.7	<0.5	<0.5	6.3	<0.5
Tb	16	18	0.6	0.6	<0.5	2.1	0.6
Th	602	608	11	6.6	7.2	94.3	6.3
U	100	85.3	3	1.6	2.1	14	1.6
W	7	<12	2	<1	1	3	<1
Yb	34	82	3	<2	<2	12	<2
Y	300	511	19	10	10	72	20
Zn	<260	500	<100	<100	<100	120	<100
Zr	26900	30000	430	<200	<200	3900	<200

whole-rock samples from heavy-mineral deposits on the Ute Mountain Ute Indian Reservation.

elements were analyzed by neutron activation except for Cu, Ga, Nb, Pb, and Y, which were analyzed by XRF. (<), below detection limit

AA–10–6	AA–10–7	AA–10–8	AA–10–9	AA–10–10	AA–10–11	AA–10–12	AA–10–13
Major oxides (percent)—Continued							
70.7	28.93	68.32	8.57	15.47	68.69	49.04	29.89
4.34	4.86	5.15	11.29	10.09	2.84	13.22	6.27
9.96	3.6	6.08	0.68	1.24	7.42	9.38	1.7
5.00	13.25	6.45	31.87	31.43	10.11	8.57	27.56
0.04	0.62	0.07	0.77	0.9	0.08	0.06	0.73
0.97	0.63	0.75	0.8	1.11	1.13	0.78	0.43
0.42	19.33	1.6	9.77	5.15	0.35	0.7	5.71
0.83	0.41	0.54	0.24	0.29	0.77	0.52	0.3
0.77	0.47	0.29	<0.01	0.06	0.88	0.74	<0.01
0.31	0.29	0.59	0.23	0.2	0.05	0.23	0.44
0.01	0.12	<0.01	0.38	0.37	0.02	0.04	0.44
93.35	72.51	89.82	64.61	66.31	92.34	83.28	73.39
Trace elements (parts per million)—Continued							
<6	<7	<2	<9	<11	<2	<10	<5
2.8	<2.0	<1.1	9	<3.0	5.5	<2.9	2.5
<.005	<.007	0.026	<.009	<.010	0.02	0.014	0.089
410	290	200	<190	320	410	470	790
<2	<2	<2	<2	<2	<2	2.1	2.5
586	723	595	1170	1010	280	1840	1100
36	53	9	86	130	29	<11	40
520	700	400	1600	1300	350	1200	840
<0.5	<1.2	<0.5	<1.5	<1.8	1.6	<1.6	<0.5
8	60	32	139	67	73	118	180
<4	<5	<2	6	<6	4	<7	<3
<26	<26	<26	73	<26	<26	86	76
86	189	87	489	362	71	555	298
3100	417	355	715	572	160	1120	652
2.4	4.1	2.7	10	6.7	1.4	13	6.5
<1	<3	<1	<4	<4	<1	<5	<1
88	108	120	192	171	47	278	156
<29	<33	<20	<43	<50	32	<46	<22
26	63	18	243	162	32	154	131
46	<20	11	<25	<29	33	<29	<13
1.2	1.2	0.7	2.3	2	2	2.1	0.7
35.4	43.5	33.9	55.2	50.8	18	59.1	42.7
<5	<10	<5	<11	<12	<5	<17	<5
36.8	42.7	31.5	76.2	59.5	16	128	60.8
32	31	13	65	53	37	70	36
7.7	8.8	11	16	14	3.9	18	12
4.2	4.7	3.8	9.2	7	1.6	13	7.7
88.5	161	94.6	353	268	62.4	567	223
15	28.7	18	62.4	51	10	81.7	41.8
6	7	5	5	6	<2	9	5
16	25	17	50	39	8	63	38
112	141	107	291	225	46	398	242
180	330	<100	320	360	140	450	180
4200	8200	3600	20500	16000	3100	27400	13000

APPENDIX—Chemical-composition data from neutron activation and x-ray fluorescence analyses of selected

[$FeTO_3$, total iron oxide expressed as Fe_2O_3. Cd, Ir, Sm, and Te not detected. Major oxides analyzed by x-ray fluorescence (XRF); trace (detection limit follows < symbol)]

Sample numbers	AA–11	AA–13	AA–14	AA–16	AA–17–1	AA–17–2	AA–17–3
			Major oxides (percent)				
SiO_2	54.59	56.78	36.75	12.42	63.95	22.68	18.91
TiO_2	0.48	8.06	4.47	12.67	0.45	8.68	5.56
Al_2O_3	0.78	3.69	1.96	2.17	7.37	2.01	1.49
$FeTO_3$	23.51	14.5	22.69	18.65	15.42	31.02	34.91
MnO	1.37	0.06	0.76	0.59	0.19	0.67	0.4
MgO	0.13	0.23	0.13	1.05	0.2	0.31	0.62
CaO	4.99	0.7	6.03	17.84	0.54	2.16	3.13
Na_2O_3	0.3	0.4	0.3	0.28	1.35	0.34	0.37
K_2O	0.03	0.18	0.04	<0.01	1.46	0.24	0.03
P_2O_5	0.1	0.58	0.34	0.41	0.09	0.27	0.23
SO_3	0.03	0.28	2.04	0.12	0.08	<0.01	0.05
Total	86.31	85.46	75.51	66.15	91.1	68.38	65.70
			Trace elements (parts per million)				
Ag	7	<5	10	12	<2	<8	<6
As	3.7	<2.7	2.7	5.1	1.7	6.5	<1.8
Au	0.04	0.059	<.005	0.029	0.011	0.019	0.012
Ba	290	350	210	450	510	410	<120
Br	<2	<2	<2	2.9	2.6	<2	<2
Ce	90	1140	947	2080	61	870	570
Co	35	<5	30	92	21	90	50
Cr	100	1000	330	1300	150	1000	750
Cs	0.7	<0.5	<0.5	<1.6	0.9	<1.2	1.6
Cu	88	89	13	279	52	29	66
Eu	1	4	3	5	<1	<4	<3
Ga	29	78	19	93	13	60	<26
Hf	7	342	173	712	3	279	180
La	54	673	452	1080	40	559	342
Lu	0.6	5.9	3.8	12	0.5	6.1	3.7
Mo	<1	<2	<1	<4	<1	<3	<2
Nb	3	178	103	299	3	146	90
Ni	30	<21	28	87	<20	67	<28
Pb	36	74	56	166	14	173	100
Rb	11	14	<15	<28	49	28	<17
Sb	0.5	1.8	1	3.9	0.5	1.8	1
Sc	12	53.9	40	71.6	16	49.1	29.9
Se	<5	<5	<5	<18	<5	<11	<5
Sm	580	68.7	47.7	105	4.3	49.2	34.3
Sr	16	30	18	54	50	46	34
Ta	0.8	14	11	24	<0.5	13	8
Tb	1.3	7.9	6.6	16	0.6	6.2	3.4
Th	9.5	284.7	162	494	7.1	210	149
U	10	41.9	32.2	87	<3.3	38	24.8
W	<1	11	5	14	<1	6	<3
Yb	3	36	23	66	3	36	24
Y	17	249	150	417	15	193	107
Zn	<100	<100	180	360	<100	320	<100
Zr	430	1400	8400	31200	390	12000	8400

whole-rock samples from heavy-mineral deposits on the Ute Mountain Ute Indian Reservation—Continued

elements were analyzed by neutron activation except for Cu, Ga, Nb, Pb, and Y, which were analyzed by XRF. (<), below detection limit

AA–17–4	AA–17–5	AA–19	AA–20	AA–21	AA–25–NW	AA–25–SE	AA–26–NW
Major oxides (percent)—Continued							
49.18	63.69	26.6	23.62	49.99	62.57	68.95	51.53
5.71	3.98	5.6	8.57	3.79	5.46	3.26	2.29
5.17	12.73	2.16	2.31	2.46	4.21	3.2	5.54
14.61	5.89	31.09	32.67	3.88	10.33	10.29	16.44
2.54	0.14	0.55	0.57	0.34	0.07	0.05	1.29
0.34	0.49	0.44	0.03	0.24	0.48	0.3	1.2
1.64	0.47	4.88	1.5	19.49	1.18	5.5	3.88
0.67	0.93	0.4	0.38	0.35	0.44	0.31	0.6
0.97	1.18	0.25	0.27	0.05	0.45	0.09	0.75
0.24	0.21	0.3	0.36	0.28	0.3	0.44	0.18
0.01	0.02	0.02	0.03	<0.01	0.75	0.13	0.07
81.08	89.73	72.29	70.31	80.87	86.24	92.52	83.77
Trace elements (parts per million)—Continued							
<7	<5	<2	<6	<5	<6	<5	<2
4.2	10	4.3	2.4	<2.3	<1.9	6.4	3.8
0.014	0.013	0.09	0.038	0.078	0.007	0.008	<.002
890	370	650	290	270	<130	220	720
2.9	4.9	<2	<2	<2	2.6	<2	2
678	523	726	1210	1380	1070	684	370
170	12	66	77	9	13	26	71
740	460	490	750	530	530	330	340
<1.2	<0.5	<0.5	<1.1	<0.5	<1.0	0.9	0.7
72	14	31	135	130	9	<60	<60
<5	<3	3	5	5	<4	<3	<2
<26	<26	<26	48	38	<26	<26	<26
194	125	186	408	304	182	84	66
411	298	373	580	772	627	430	200
3.7	3	3.9	7.3	5.9	5.2	2.4	2.5
<3	<1	<1	<2	<3	<3	<1	<1
102	72	106	139	136	148	103	48
100	<22	49	48	<23	<29	<22	51
53	17	86	136	46	23	<19	<19
<22	35	13	<19	<14	<18	<13	25
1.6	1.6	1.5	1.6	0.5	0.8	0.8	0.6
30.3	30	34	47.2	30.6	42.4	40.2	28.2
<11	<5	<5	<11	<5	<5	<5	<5
44.7	32.5	37.3	69.1	89.5	55.7	35	22.7
48	35	35	62	32	24	12	27
8.9	6.1	8.9	12	12	13	20	4.5
5.9	4.4	5.2	10	9.4	6.6	3.6	2.8
174	112	150	318	325	223	142	67.4
30.1	20	31.4	59.4	43.4	31.1	18	15
6	9	5	9	<6	9	221	<2
20	18	22	42	37	32	17	16
180	106	139	250	261	169	90	85
<230	160	160	250	<100	210	150	240
8400	5200	8500	18000	12000	8000	3700	2900

APPENDIX—Chemical-composition data from neutron activation and x-ray fluorescence analyses of selected Continued

[$FeTO_3$, total iron oxide expressed as Fe_2O_3. Cd, Ir, Sm, and Te not detected. Major oxides analyzed by x-ray fluorescence (XRF); trace (<), below detection limit (detection limit follows < symbol)]

Sample numbers	AA–26–SE	AA–27	AA–28	AA–30	AA–36–NW	AA–36–SE	AA–37
Major oxides (percent)							
SiO_2	21.76	66.72	30.79	48.15	14.89	15.02	67.47
TiO_2	21.89	5.58	7.72	10.68	5.83	5.16	6.25
Al_2O_3	7.7	3.52	2.32	1.41	1.34	1.59	5.48
$FeTO_3$	10.82	10.37	28.3	16.28	23.71	28.21	7.95
MnO	0.19	0.11	0.97	0.09	0.27	0.41	0.51
MgO	1.52	0.63	0.3	0.13	0.17	0.25	0.78
CaO	6.31	1.94	0.99	1.03	20.95	17.09	0.62
Na_2O	0.31	0.37	0.47	0.36	0.32	0.34	0.36
K_2O	<0.01	0.15	0.42	<0.01	0.01	0.1	0.05
P_2O_5	0.61	0.22	0.26	0.55	0.34	0.29	0.2
SO_3	0.18	0.08	<0.01	1.61	0.15	0.16	0.01
Total	71.29	89.69	72.54	80.29	67.98	68.62	89.68
Trace elements (parts per million)							
Ag	<7	<2	<5	<2	<6	<4	<6
As	<3.6	4.4	12	2.7	29	6.1	<1.3
Au	0.025	0.039	0.059	0.041	0.085	<.004	0.059
Ba	<140	130	480	1100	870	500	360
Br	<2	<2	<2	<2	7.1	10	<2
Ce	3890	1260	856	2350	949	645	1150
Co	23	10	82	<5	88	66	20
Cr	2230	480	920	900	1200	780	640
Cs	<1.1	<0.5	1.3	<0.5	<0.5	1	<1.0
Cu	471	117	<60	159	78	141	98
Eu	10	3	4	2	<3	3	6
Ga	412	65	<26	111	<26	40	67
Hf	1470	360	310	770	342	206	324
La	2530	588	490	1250	559	381	577
Lu	29.2	6.1	5.7	12	7	4.5	6.9
Mo	<5	<1	<2	<1	<2	<1	<3
Nb	672	162	126	300	112	101	162
Ni	<33	<20	57	<20	<25	<20	<29
Pb	239	21	133	85	85	81	59
Rb	<19	25	14	<11	<15	<12	<18
Sb	1	0.8	2.1	1.2	3.1	1.3	0.7
Sc	119	39.6	48.9	62.2	50.5	34.4	43.7
Se	<11	<5	<5	<5	<5	<5	<10
Sm	265	65	55.5	128	63.5	36.4	63.9
Sr	105	19	50	45	34	33	30
Ta	42	14	10	26	13	7.9	13
Tb	31	8.5	7	17	8.3	5	8.2
Th	1080	286	223	559	284	163	255
U	180	42.1	38.2	82.5	48.1	28.9	41.5
W	<9	7	<5	10	62	3	7
Yb	150	33	35	65	39	25	44
Y	1205	255	194	475	199	146	300
Zn	270	<100	330	<100	570	240	270
Zr	59800	16000	13000	36300	15000	8600	14000

whole-rock samples from heavy-mineral deposits on the Ute Mountain Ute Indian Reservation—

trace elements were analyzed by neutron activation except for Cu, Ga, Nb, Pb, and Y, which were analyzed by XRF.

AA–38	AA–39	AA–40	AA–41	AA–43	AA–44	FA–1
Major oxides (percent)—Continued						
56.84	56.05	28.35	15.44	27.42	13.95	54.65
10.4	14	16.49	9.3	7.27	10.29	0.51
9.95	6.74	9.1	1.39	3.04	1.36	3.47
6.72	6.06	15.93	31.84	28.26	30.81	23.76
0.09	0.12	0.16	0.61	0.7	0.55	0.44
0.86	1	2.39	1.05	0.91	0.73	0.42
0.51	0.97	1.48	6.29	2.67	6.91	1.35
0.42	0.38	0.29	0.26	0.31	0.26	0.55
0.41	0.32	0.3	<0.01	0.16	<0.01	0.68
0.35	0.52	0.68	0.36	0.4	0.31	0.06
0.09	0.01	<0.01	<0.01	0.02	0.02	0.03
86.64	86.17	75.17	66.54	71.16	65.10	85.92
Trace elements (parts per million)—Continued						
<8	<7	<8	<6	<7	<8	<2
3.6	4.5	<3.2	<2.7	<1.8	<3.6	<1.4
0.041	0.08	0.021	0.049	0.11	0.06	0.015
270	430	380	370	550	390	400
3	3.1	2.4	<2	<2	<2	<2
1340	1620	1870	1060	791	990	82
17	17	44	67	43	55	53
1000	1200	1500	1100	810	940	170
1.6	<1.1	<1.2	1.2	<1.1	<1.3	0.9
23	52	63	137	60	175	98
<5	4	5	<3	<4	<5	<1
65	85	76	32	49	25	7
397	511	388	363	189	314	4
764	946	1140	633	463	623	71
8.7	10	10	6.8	4.8	6.4	0.5
<3	<3	<4	<4	<2	<3	<1
218	331	324	166	135	193	6
<36	<30	<34	<27	<30	<35	40
68	113	89	140	104	195	33
<21	<18	<20	<16	<18	<21	28
2	2.2	2.6	1.7	1.5	2.3	0.4
68.1	87.2	93.9	54	46.9	51	15
<12	<5	<10	<5	<5	<12	<5
80.5	97.1	107	63.1	46.3	67.8	637
40	46	34	38	30	39	33
16	23	26	14	11	16	0.5
10	12	13	8.8	5.3	9	1.3
274	324	295	243	149	275	8.6
52	59.4	51.6	42.8	29.1	16.6	31.4
12	13	14	<7	6	5	<3
48	65	62	40	28	33	3
359	469	348	260	177	263	22
300	190	500	330	370	320	190
17000	20800	15000	16000	8400	14000	<200

Geologic Studies of the Ute Mountain Ute Indian Reservation

U.S. GEOLOGICAL SURVEY BULLETIN 2061

This volume was published as separate chapters A and B

UNITED STATES GOVERNMENT PRINTING OFFICE, WASHINGTON : 1994

U.S. DEPARTMENT OF THE INTERIOR
BRUCE BABBITT, Secretary

U.S. GEOLOGICAL SURVEY
Gordon P. Eaton, Director

For sale by U.S. Geological Survey, Map Distribution
Box 25286, MS 306, Federal Center
Denver, CO 80225

CONTENTS

SELECTED SERIES OF U.S. GEOLOGICAL SURVEY PUBLICATIONS

Periodicals

Earthquakes & Volcanoes (issued bimonthly).
Preliminary Determination of Epicenters (issued monthly).

Technical Books and Reports

Professional Papers are mainly comprehensive scientific reports of wide and lasting interest and importance to professional scientists and engineers. Included are reports on the results of resource studies and of topographic, hydrologic, and geologic investigations. They also include collections of related papers addressing different aspects of a single scientific topic.

Bulletins contain significant data and interpretations that are of lasting scientific interest but are generally more limited in scope or geographic coverage than Professional Papers. They include the results of resource studies and of geologic and topographic investigations; as well as collections of short papers related to a specific topic.

Water-Supply Papers are comprehensive reports that present significant interpretive results of hydrologic investigations of wide interest to professional geologists, hydrologists, and engineers. The series covers investigations in all phases of hydrology, including hydrology, availability of water, quality of water, and use of water.

Circulars present administrative information or important scientific information of wide popular interest in a format designed for distribution at no cost to the public. Information is usually of short-term interest.

Water-Resources Investigations Reports are papers of an interpretive nature made available to the public outside the formal USGS publications series. Copies are reproduced on request unlike formal USGS publications, and they are also available for public inspection at depositories indicated in USGS catalogs.

Open-File Reports include unpublished manuscript reports, maps, and other material that are made available for public consultation at depositories. They are a nonpermanent form of publication that may be cited in other publications as sources of information.

Maps

Geologic Quadrangle Maps are multicolor geologic maps on topographic bases in 7 1/2- or 15-minute quadrangle formats (scales mainly 1:24,000 or 1:62,500) showing bedrock, surficial, or engineering geology. Maps generally include brief texts; some maps include structure and columnar sections only.

Geophysical Investigations Maps are on topographic or planimetric bases at various scales, they show results of surveys using geophysical techniques, such as gravity, magnetic, seismic, or radioactivity, which reflect subsurface structures that are of economic or geologic significance. Many maps include correlations with the geology.

Miscellaneous Investigations Series Maps are on planimetric or topographic bases of regular and irregular areas at various scales; they present a wide variety of format and subject matter. The series also includes 7 1/2-minute quadrangle photogeologic maps on planimetric bases which show geology as interpreted from aerial photographs. The series also includes maps of Mars and the Moon.

Coal Investigations Maps are geologic maps on topographic or planimetric bases at various scales showing bedrock or surficial geology, stratigraphy, and structural relations in certain coal-resource areas.

Oil and Gas Investigations Charts show stratigraphic information for certain oil and gas fields and other areas having petroleum potential.

Miscellaneous Field Studies Maps are multicolor or black-and-white maps on topographic or planimetric bases on quadrangle or irregular areas at various scales. Pre-1971 maps show bedrock geology in relation to specific mining or mineral-deposit problems; post-1971 maps are primarily black-and-white maps on various subjects such as environmental studies or wilderness mineral investigations.

Hydrologic Investigations Atlases are multicolored or black-and-white maps on topographic or planimetric bases presenting a wide range of geohydrologic data of both regular and irregular areas; the principal scale is 1:24,000, and regional studies are at 1:250,000 scale or smaller.

Catalogs

Permanent catalogs, as well as some others, giving comprehensive listings of U.S. Geological Survey publications are available under the conditions indicated below from USGS Map Distribution, Box 25286, Building 810, Denver Federal Center, Denver, CO 80225. (See latest Price and Availability List.)

"Publications of the Geological Survey, 1879-1961" may be purchased by mail and over the counter in paperback book form and as a set microfiche.

"Publications of the Geological Survey, 1962-1970" may be purchased by mail and over the counter in paperback book form and as a set of microfiche.

"Publications of the U.S. Geological Survey, 1971-1981" may be purchased by mail and over the counter in paperback book form (two volumes, publications listing and index) and as a set of microfiche.

Supplements for 1982, 1983, 1984, 1985, 1986, and for subsequent years since the last permanent catalog may be purchased by mail and over the counter in paperback book form.

State catalogs, "List of U.S. Geological Survey Geologic and Water-Supply Reports and Maps For (State)," may be purchased by mail and over the counter in paperback booklet form only.

"Price and Availability List of U.S. Geological Survey Publications," issued annually, is available free of charge in paperback booklet form only.

Selected copies of a monthly catalog "New Publications of the U.S. Geological Survey" is available free of charge by mail or may be obtained over the counter in paperback booklet form only. Those wishing a free subscription to the monthly catalog "New Publications of the U.S. Geological Survey" should write to the U.S. Geological Survey, 582 National Center, Reston, VA 22092.

Note.–Prices of Government publications listed in older catalogs, announcements, and publications may be incorrect. Therefore, the prices charged may differ from the prices in catalogs, announcements, and publications.